Toward a better understanding of the basis of the molecular mimicry of polysaccharide antigens by peptides: *the example of shigella flexneri 5A*

M.-J. Clement, A. Fortune, A. Phalipon, V. Marcel-Peyre, C. Simenel, A. Imberty, M. Delepierre, Laurence A. Mulard

HAL Id: pasteur-01115171
https://pasteur.hal.science/pasteur-01115171

Submitted on 23 Dec 2022

Toward a Better Understanding of the Basis of the Molecular Mimicry of Polysaccharide Antigens by Peptides
THE EXAMPLE OF SHIGELLA FLEXNERI 5A*[S]

Marie-Jeanne Clément[‡]**, Antoine Fortuné**[§]**, Armelle Phalipon**[¶]**, Véronique Marcel-Peyre**[¶]**, Catherine Simenel**[‡]**, Anne Imberty**[||]**, Muriel Delepierre**[‡1]**, and Laurence A. Mulard**[**]

From the [‡]*Unité de RMN des Biomolécules, URA CNRS 2185, Institut Pasteur,* [**]*Unité de Chimie Organique, URA CNRS 2128, Institut Pasteur,* [¶]*Unité de Pathogénie Microbienne Moléculaire, Institut Pasteur, 28 Rue du Dr. Roux, 75724 Paris Cedex 15,* [§]*DPM UMR5063 UJF/CNRS, 5 Avenue de Verdun 38240 Meylan, France, and the* [||]*CERMAV-CNRS (affiliated with Université Joseph Fourier) , 38041 Grenoble BP53, Cedex 09, France*

Protein conjugates of oligosaccharides or peptides that mimic complex bacterial polysaccharide antigens represent alternatives to the classical polysaccharide-based conjugate vaccines developed so far. Hence, a better understanding of the molecular basis ensuring appropriate mimicry is required in order to design efficient carbohydrate mimic-based vaccines. This study focuses on the following two unrelated sets of mimics of the *Shigella flexneri* 5a O-specific polysaccharide (O-SP): (i) a synthetic branched pentasaccharide known to mimic the average solution conformation of *S. flexneri* 5a O-SP, and (ii) three nonapeptides selected upon screening of phage-displayed peptide libraries with two protective murine monoclonal antibodies (mAbs) of the A isotype specific for *S. flexneri* 5a O-SP. By inducing anti-O-SP antibodies upon immunization in mice when appropriately presented to the immune system, the pentasaccharide and peptides p100c and p115, but not peptide p22, were qualified as mimotopes of the native antigen. NMR studies based on transferred NOE (trNOE) experiments revealed that both kinds of mimotopes had an average conformation when bound to the mAbs that was close to that of their free form. Most interestingly, saturation transfer difference (STD) experiments showed that the characteristic turn conformations adopted by the major conformers of p100c and p115, as well as of p22, are clearly involved in mAb binding. These latter experiments also showed that the branched glucose residue of the pentasaccharide was a key part of the determinant recognized by the protective mAbs. Finally, by using NMR-derived pentasaccharide and peptide conformations coupled to STD information, models of antigen-antibody interaction were obtained. Most interestingly, only one model was found compatible with experimental data when large O-SP fragments were docked into one of the mIgA-binding sites. This newly made available system provides a new contribution to the understanding of the molecular mimicry of complex polysaccharides by peptides and short oligosaccharides.

Bacterial capsular polysaccharides (CPS)[2] and lipopolysaccharides (LPS) are known to be important virulence factors and major targets of the protective immune response of the host (1). Several polysaccharide vaccines such as those targeting *Streptococcus pneumoniae*, *Neisseria meningitidis,* or *Salmonella typhi* were proven efficient in adults and are thus commercially available. Their ineffectiveness in infants has been successfully circumvented with the licensing of polysaccharide:protein conjugates such as those targeting *Haemophilus influenzae* b, *S. pneumoniae,* and *N. meningitidis* group C infections (2). A possible alternative may derive from the use of accurate synthetic mimics of the bacterial polysaccharide antigens. This innovative approach has been mostly developed along two lines, including the use of either synthetic oligosaccharides or peptides mimicking the carbohydrate determinants recognized by anti-carbohydrate monoclonal antibodies (mAb) conferring protection in experimental models of infection. Indeed, semi-synthetic glycoconjugates incorporating oligosaccharides mimicking fragments of bacterial polysaccharide antigens were shown to be highly immunogenic in mice (3–5). The "proof of concept" was recently demonstrated in humans with the efficacy of such a semi-synthetic glycoconjugate in protecting against *H. influenzae* b infection (6).

However, access to the required carbohydrate haptens is often a roadblock. Therefore, besides the investigation of anti-idiotype antibody (7), expanding the concept of mimicry led in the recent past to extensive exploring of the potential mimicking of polysaccharide and/or complex oligosaccharide antigens by peptides (8–10). These peptide mimotopes, *i.e.* peptide mimics inducing an anti-carbohydrate antibody response upon immunization, have been proposed as potential surrogate antigens of carbohydrates in vaccine development (10). Indeed, because of their ease of manufacture and their intrinsic immunogenic properties, peptide mimotopes may have greater advantage over complex carbohydrate haptens issued from bacterial cell cultures or low yielding multistep syntheses. However, not all peptide mimics of carbohydrate antigens behave as mimotopes. Despite the large number of known peptide mimics, only few peptide mimotope-based experimental vaccines have been reported so far (11–16).

It is believed that a better understanding of the molecular basis of peptide-carbohydrate mimicry could help the rational design of potent peptide mimotope-based vaccines. In particular, whether mimicry is
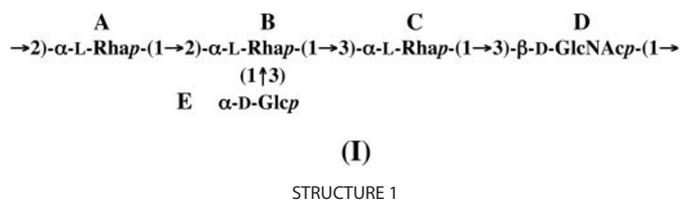

Peptide Mimics of S. flexneri 5a Polysaccharide Antigen

```
          A               B               C               D
→2)-α-L-Rhap-(1→2)-α-L-Rhap-(1→3)-α-L-Rhap-(1→3)-β-D-GlcNAcp-(1→
                              (1↑3)
                          E    α-D-Glcp
```

(I)

STRUCTURE 1

structural, functional, or both remains an unsolved question (9, 17–19). Available x-ray data of carbohydrate-protein and of the corresponding peptide mimotope-protein complexes along with information on the thermodynamics of peptide mimic-protein binding are somewhat scarce (17, 20, 21). Thus to date, although analysis of the topography of ligand-receptor complementarity may be performed by a variety of methods, available knowledge on the molecular features of peptide-carbohydrate mimicry mostly relies on data obtained from NMR and molecular modeling studies as reviewed recently (22).

By aiming to prevent *S. flexneri* bacterial infections, during the past few years we investigated the development of synthetic mimics of the major protective *S. flexneri* antigen. *S. flexneri*, a Gram-negative bacillus, is responsible for the endemic form of shigellosis, a human dysenteric syndrome causing a high mortality rate in infants, particularly in developing countries (23). The disease, characterized by bacterial invasion of the human colonic mucosa, leads to acute inflammation and subsequent massive tissue destruction (24). Protection induced upon infection is serotype-specific (24), pointing to the O-specific polysaccharide moiety (O-SP) of the bacterial LPS as the major target for protective immunity. In line with the success of the CPS-protein conjugate vaccines, protein conjugates of detoxified *S. flexneri* 2a LPS, the prevalent serotype in humans, were shown to be safe and immunogenic both in adults and young children (25). More recently, we developed fully synthetic glycoconjugates as well as promising neoglycoproteins exposing well designed synthetic saccharidic haptens mimicking *S. flexneri* 2a O-SP as potential vaccines against the homologous infection (26, 27).[3] Alternatively, we also investigated the potential of peptide mimotopes, and we reported the first example of immunogenic mimicry of carbohydrates by peptides identified by screening of phage-displayed nonapeptide libraries with two protective mAbs of the A isotype (mIgA) specific for *S. flexneri* serotype 5a, mIgA C5, and mIgA I3 (28). Among the 19 peptide sequences selected upon screening with mIgA I3, p100c (YKPLGALTH) and p115 (KVPPWARTA, also interacting with mIgA C5) only induce anti-O-SP antibodies in mice upon immunization with the corresponding phage particles. Most interestingly, the mimotopes share no obvious consensus sequence and do not cross-react with one another. However, as often reported by others (29, 30), their amino acid sequences contain aromatic and hydrophobic residues but also amino acids having cyclic side chains, including at least one proline.

Besides, based on a combination of NMR and molecular modeling studies, we proposed a conformational model for the *S. flexneri* 5a O-SP whose biological repeating unit is the branched pentasaccharide I (Structure 1) (31). Study of both the antigenicity and the conformation of the four synthetic frame-shifted pentasaccharides corresponding to pentasaccharide I (32) suggested that the DA(E)BC sequence is the structure that best mimics the native O-SP antigen (33). More recently, the pentasaccharide DA(E)BC was shown to act as a mimotope.[4]

Here we report the antigenicity and the NMR findings on the preferred conformation of p100c and p115 peptide mimotopes both in their free and mIgA-bound forms. Analysis was also performed using peptide p22 (KRHFLSQRQ, mIgA C5- and mIgA I3-specific), one of the 17 nonimmunogenic peptides selected during the original screening (28). Antibody-bound conformations and epitope mapping were derived from transferred NOE (trNOE) (34, 35) and saturation transfer difference (STD) experiments (36), respectively. The conformational preferences observed for the peptides were tentatively related to those derived from NMR and molecular modeling analysis of the DA(E)BC-mIgA complexes that led to a theoretical model of the recognition of *S. flexneri* 5a O-SP by mIgA I3. This contribution adds to the few reports investigating molecular mimicry by analyzing both peptide mimic-mAb and carbohydrate-mAb recognition features (37–39).

EXPERIMENTAL PROCEDURES

Material—Selected nonapeptides p100c (YKPLGALTH), p115 (KVPPWARTA), and p22 (KRHFLSQRQ) were purchased from Synthem (Saint-Christol-Les-Alès, France). The peptide p100c was further cyclized in the Unité de Chimie Organique at the Pasteur Institute. Pentasaccharide DA(E)BC was used in its methyl glycoside form DA(E)BC-OMe (40). mAb mIgA C5 and mIgA I3 were prepared as described previously (41).

Inhibition ELISA—Characterization of the oligosaccharide determinant recognized by the mIgA was performed by measuring the mIgA-oligosaccharide interaction as follows. First of all, a standard curve was established for each mIgA tested. Different concentrations of the mAb were incubated overnight at 4 °C on microtiter plates coated with purified *S. flexneri* 5a LPS at a concentration of 5 μg/ml in carbonate buffer, pH 9.6, and subsequently incubated with 1% PBS/BSA for 30 min at 4 °C. After washing with PBS/Tween 20 (0.05%), alkaline phosphatase-conjugated anti-mouse IgA was added at a dilution of 1:5,000 (Sigma) for 1 h at 37 °C. After washing with PBS/Tween 20 (0.05%), the substrate was added (12 mg of *p*-nitrophenyl phosphate in 1.2 ml of 1 M Tris-HCl buffer, pH 8.8, and 10.8 ml of 5 M NaCl). Once the color developed, the plate was read at 405 nm (Dynatech MR 4000 microplate reader). A standard curve A = f([Ab]) was fitted to the quadratic equation $Y = aX^2 + bX + c$, where Y is the absorbance and X is the Ab concentration. Correlation factor (r^2) of 0.99 was routinely obtained.

Then the amount of oligosaccharides giving 50% inhibition of mIgA binding to LPS (IC_{50}) was determined as follows. Each mIgA at a given concentration (chosen as the minimal concentration of Ab which gives the maximal absorbance on the standard curve) was incubated overnight at 4 °C with various concentrations of each of the oligosaccharides to be tested, in 1% PBS/BSA. Measurement of unbound mIgA was performed as described above using microtiter plates coated with purified LPS from *S. flexneri* 5a, and the mAb concentration was deduced from the standard curve.

The recognition capacity of anti-LPS mIgA for LPS was determined as described above using various concentrations of LPS that were incubated in solution overnight at 4 °C with the predefined concentration of each mIgA. IC_{50} was defined as the concentration of oligosaccharides required to inhibit 50% of mIgA binding to LPS.

NMR Spectroscopy—All ^{1}H NMR experiments were recorded at 298 K on a Varian Unity Inova spectrometer operating at ^{1}H frequencies of 500 MHz. ^{1}H chemical shifts were given relative to an external standard of 4,4-dimethyl-4-silapentane sodium sulfonate at 0 ppm.

Free Peptides—The samples were prepared in 90% H_2O and 10% D_2O at pH 5 for p115 and p100c and at pH 6.5 for p22. The solution concentrations were about 10, 3, and 8 mM for p115, p100c, and p22, respectively. DQF-COSY (42), TOCSY (43), and ROESY (44) experiments were recorded with 512 increments and 16 scans at 298 K. The TOCSY

---

and ROESY experiments were acquired using a mixing time of 80 and 400 ms, respectively. Water suppression was performed using the WATERGATE pulse sequence (45). All NMR spectra were collected in the phase-sensitive mode using the States-Haberkorn method (46).

Ligand-Antibody Interactions—Shigemi tubes were used for all samples. In order to prepare NMR samples of pentasaccharide DA(E)BC-OMe in the presence of the antibodies mIgA C5 and mIgA I3, mAbs were concentrated after repeated cycles of exchange with D_2O buffer (50 mM deuterated sodium phosphate, 100 mM NaCl, pH 6.5) in Amicon Centriprep-10 concentrators. trNOE experiments (34, 35, 47) performed on different pentasaccharide:binding site ratios (5:1, 10:1, 15:1, 20:1, and 30:1) showed that the most favorable ratio for trNOE was 20:1. So the final samples were prepared with 3.75 μM antibody and 0.3 mM pentasaccharide in 380 μl of the above mentioned D_2O buffer. trNOE, trROE, and STD experiments (36) on pentasaccharide DA(E)BC-OMe in the presence of mIgA C5 and mIgA I3 were recorded at 500 and 600 MHz, respectively. trNOE experiments were performed with mixing times of 100, 150, 250, 300, and 400 ms at 303 K to obtain build-up curves and trROE with a mixing time of 400 ms.

The conformation of the free peptides was studied at pH 5. However, with this pH value being close to the isoelectric points of the mIgAs, a study of peptides in their bound conformation was performed at pH 6.5 to avoid precipitation of the mAb. Similarly to the DA(E)BC-mIgA complexes, a peptide:antibody-binding site ratio of 20:1 was used (0.3 mM:3.75 μM). trNOE experiments were performed with mixing times of 100, 150, 250, 300, and 400 ms. To be sure that the observed negative cross-peaks were real trNOEs, NOESY spectra were recorded under the same pH, temperature, and concentration values with the peptides alone. Furthermore, to discard any impact on NOE effects of viscosity increase as a result of the mAb presence, a NOESY spectrum ($\tau_m = 200$ ms) of p115 was registered in the presence of BSA at the same concentration ratio as that used with the mIgAs. Because no negative NOE cross-peaks were observed in either case, it was assumed that the negative NOEs observed in the presence of mIgA were trNOEs.

Selective saturation of antibody resonances were performed for all STD-NMR experiments at 0.3 ppm (30 ppm for reference spectra) using a series of 40 gaussian-shaped pulses (50- and 10-ms delay between pulses, excitation width $\gamma B_1/2\pi$, approximately 50 Hz) for a total saturation time of 2.4 s. The one-dimensional STD spectra were recorded with 4096 scans at 288 and 298 K for the pentasaccharide and the peptides, respectively. Subtraction of saturated spectra from reference spectra was obtained by phase cycling (36). For DA(E)BC-OMe, two STD-TOCSY experiments (48) were recorded with selective saturation at 0.3 and 30 ppm, respectively. Differences between the two spectra were performed using the VNMR software. No attempt here was made to quantify STD-NMR intensities, as it is known that these exhibit a complex dependence on relaxation times, correlation times, exchange rates, and on binding site proton density. Indeed, only when short saturation times are used, *i.e.* less than 1 s, can intensities reflect ligand proton-protein proton distances (37). Here the saturation time of 2.4 s prevented us from quantitative analysis.

Distance and Angle Constraints—The cross-peak volumes from trNOESY and trROESY experiments of the pentasaccharide in the presence of mIgAs were measured with the VNMR software. Distances between neighboring protons were calculated by the usual $1/r^6$ NOE/distance relationship (49). NOE-derived and trROE distances were obtained from initial NOE build-up rates, which were calculated by NOE volumes fitting during different mixing times. The intra-residue distance of 2.52 Å between the H-1 and H-2 protons of the α-L-rhamnopyranosyl unit B was used as a reference for distance calibration.

Distance constraints of free peptides were obtained from the ROESY spectrum run at 298 K with a 400-ms mixing time. For peptides in the presence of mIgA, distance constraints were obtained from the trNOESY spectra run at 298 K with a 200-ms mixing time. NOE intensities were evaluated from the height of the cross-peaks. For structure calculations, upper limit distances of 2.8, 3.5, and 5 Å were used for strong, medium, and weak NOEs, respectively (50). The $^3J_{NH-H\alpha}$ values were used to restrain Φ angles as follows: for $^3J > 9$ Hz, $-155° < \Phi < -85°$; for 8 Hz $< ^3J <9$ Hz, $-175° < \Phi < -65°$; for 5 Hz $< ^3J <7$ Hz, $-105° < \Phi < -55°$; for $^3J <5$ Hz, $-90° < \Phi < -40°$ (51).

Structure Calculations—Structure calculations of free and bound peptides were run on a Silicon Graphics work station using the standard protocol of the DYANA program (52). A total of 100 structures were calculated using the torsion angle dynamics protocol. The structures were sorted according to the final value of the target function, and the 20 best structures were analyzed in terms of distance and angle violations. Of these 20 structures, the 10 best structures were visualized by using MOLMOL (53).

Homology Modeling of the IgA I3 Fab Fragment and Docking—The search for structures with sequences similarities was performed with Blast (54) on sequences of all proteins with known three-dimensional structure in the Protein Data Bank (55). Five structures of interest were downloaded and used as template by the Composer program for the building of VL and VH chains of IgA I3 (56).

The Tripos force field (57) option of the Sybyl program (SYBYL) was used to minimize the energy of the resulting model whose stereochemical features were validated with the PROCHECK program (58).

The Autodock3 program (59) was used for docking oligosaccharides and peptides in the binding site of modeled IgA I3 Fab. Because the goal was to model the behavior of the O-SP, calculations were performed on the largest possible fragment compatible with the limitations of the software, in that case a nonasaccharide. The 9-carbohydrate residue fragment was thus chosen as BCDA(E)BCDA in which the key pentasaccharide DA(E)BC is flanked by two residues on each side. The two conformations that were shown previously to correspond to helical shapes of the O-SP (33) were used as starting models. Hydroxyl and *N*-acetyl bonds were considered as flexible, whereas glycosidic bonds were considered as rigid to keep the helical conformation, resulting in 28 degrees of freedom. AMBER force field charges were assigned to all protein atoms, and partial charges were assigned to the atoms according to the PIM force field (60). Grids of probe atom interaction energies and electrostatic potential were generated around the whole protein by the AutoGrid program present in Autodock3 with a spacing of 0.5 Å. All probes were placed arbitrarily at a distance of 10 Å from the protein surface, and their exocyclic torsion angles were allowed to rotate freely. For each monosaccharide, one job of 240 docking runs was performed using a population of 100 individuals and an energy evaluation number of 10×10^6. Clustering of solutions was done by root mean square fitting (<1 Å). The best solution of each cluster was used to propagate the helices to 20 residues while keeping the conformations determined previously (33). Twenty different conformers of the p100c peptide were also docked in the mIgA I3 Fab-binding site using the rigid body approach of the Autodock3 program. For each of them, one docking run was performed using a population of 100 individuals and an energy evaluation number of 0.75×10^6.

RESULTS

Antigenicity of the Ligands Used in the Study—The binding of the synthetic nonapeptides p100c, p115, and p22 (28) and synthetic pentasaccharide DA(E)BC-OMe (32) to mIgA I3 and mIgA C5 was evalu-

ated by inhibition ELISA to determine the concentration of ligands inhibiting 50% of mIgA binding to LPS (IC_{50} value). Because of the multivalency of both the mIgAs (dimeric mAb, thus four binding sites) and LPS, the IC_{50} value does not reflect the true binding affinity but allows relative comparison of the ligand recognition by the mIgAs. In agreement with the low affinity of mAb for carbohydrate antigens, an IC_{50} value close to 25 mM was observed for the interaction of DA(E)BC-OMe with each of the mIgAs.

IC_{50} values for recognition of the mimotopes by mIgAs revealed that p100c was better recognized by mIgA I3 (IC_{50} = 75 ± 29 μM) than by

mIgA C5 (IC_{50} >1000 μM). In contrast, p115 was better recognized by mIgA C5 (IC_{50} = 197 ± 39 μM) than by mIgA I3 (IC_{50} >1000 μM). Most interestingly, p22 exhibited a higher IC_{50} value for both mIgAs (70 ± 11 μM and 0.03 ± 0.01 μM for mIgA I3 and mIgA C5, respectively) than those measured for p100c and p115.

NMR Parameters for the Free Peptide—Peptide proton chemical shifts were assigned following standard procedures (50). The peptide conformations were probed through analysis of proton chemical shifts, three bond $^3J_{\text{NH-H}\alpha}$ coupling constants, and proton-proton dipolar interactions observed in the ROESY spectra. Dihedral angles and distance constraints deduced from these data were then used to model the averaged solution structure of each peptide analyzed with the DYANA program (52).

Peptide 115 (KVPPWARTA)—The NMR spectrum revealed that p115 displayed four different conformers as a result of the *cis-trans* isomerization of the amide bonds involving the two sequential prolines, Val^2–Pro^3 and Pro^3–Pro^4, respectively. Based on signal intensities, it was estimated that the major conformer represented 80% of the different species, whereas the three other forms altogether made up for the remaining 20%. Because no information was available for the conformer recognized upon selection from the phage displayed peptide library, structural analysis was conducted for this major conformer only. Chemical shifts and three bond $^3J_{\text{NH-H}\alpha}$ coupling constants are reported in Table 1. Significant deviations from random coil values are only observed for the H-α protons of Pro^3 and Pro^4, whereas all three bond $^3J_{\text{NH-H}\alpha}$ coupling constants are those expected for flexible peptides. Inter-residue dipolar interactions observed in the ROESY experiment between the H-α of the residue preceding a proline and the H-δ proton of the proline indicates that both Pro^3 and Pro^4 adopt a *trans*-conformation in the peptide major conformer. In addition to standard sequential interactions, several medium range interactions were also observed between side chain protons of Val^2, Pro^3, and Pro^4 and the CH$_3$-β protons of Ala^6 (Fig. 1). These ROE connectivities were used as distance constraints to model the conformation of the p115 major conformer using the DYANA program. The 10 best structures, *i.e.* with the lowest

TABLE 1
^{1}H chemical shifts of the *trans-trans*-isomer of p115 in H$_2$O/D$_2$O (90/10), pH 5.1 and 298 K

Chemical shifts measured in ppm with an accuracy of ±0.01 ppm are referenced to external 4,4-dimethyl-4-silapentane sodium sulfonate (δ_H 0.00).

Residue	H$_N$	H$_\alpha$	H$_\beta$	Others
Lys^1	ND^a	4.02 −0,30^b	1.84	H-γ1.38 H-δ1.66 H-ϵ2.96 H-ζ ND
Val^2	8.54 (ND)	4.41	2.02	H-γ0.94−0.89
Pro^3		4.52 −0,21	1.97−1.05	H-γ1.71−1.85 Hδ3.81−3.51
Pro^4		4.28 −0,14	2.24−1.91	H-γ1.99 H-δ3.69−3.44
Trp^5	7.31 (6.80)^c	4.61 −0,05	3.35−3.26	H-δ17.24 H-ζ37.16 H-ϵ110.26
Ala^6	7.64 (6.60)	4.27 −0,05	1.15	
Arg^7	8.00 (6.70)	4.28 −0,06	1.82−1.60	H-γ1.72 H-δ3.17 H-η7.16−6.65
Thr^8	8.17 (8.10)	4.30 −0,05	4.23	H-γ1.17
Ala^9	7.97 (6.60)	4.11	1.32	

^{a} ND indicates not determined.
^{b} Data in italics are the difference between the Hα chemical shifts of the residues of the peptide and those of the same residues in nonstructured peptides GGXAGG or GGXPGG (90).
^{c} Data in parentheses are $^3J_{\text{HN,H}\alpha}$ coupling constants (in Hz ± 0.2 Hz) measured from the one-dimensional spectrum.
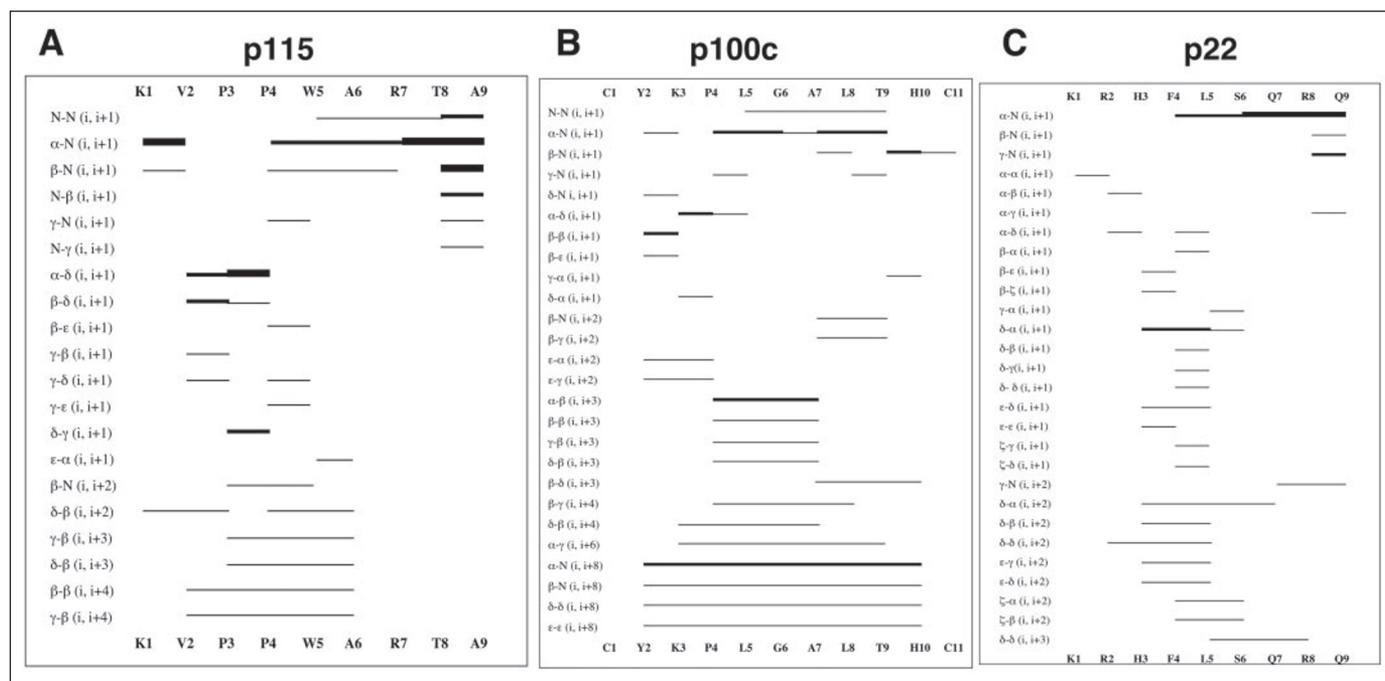

FIGURE 1. **^{1}H-^{1}H NOE connectivities observed for the major conformers of peptides.** *A,* p115 *trans-trans*-isomer; *B,* p100c *trans*-isomer; *C,* p22. The intensity of the NOE cross-peak is indicated by the *thickness* of the *lines* (weak, –; medium, —; strong ■).

energy function, showed that p115 adopts a rather organized conformation comprising residues Pro[3] to Arg[7], whereas the N- and C-terminal ends are quite flexible (Fig. 2) as expected for peptides of this size. Based on C-α_i–C-α_{i+3} distances as well as on Φ and Ψ angle values (Table 2), the conformation of the Pro[3]–Arg[7] fragment can be described as two sequential β-turns, a nonclassified one for PPWA and a type I β-turn for PWAR (61, 62).

Peptide 100c (CYKPLGALTHC)—Selected from a library displaying nonapeptides flanked by two cysteines (pVIII-9aa Cys) (28), synthetic p100c was chemically converted into its cyclic form. NMR data showed that in solution p100c existed as a 9:1 equilibrium between two conformers resulting from the *cis-trans*-isomerization of the amide bond between Lys[3] and Pro[4]. Again, despite the lack of information on the p100c-mIgA I3 recognition, only the major conformer was analyzed (Table 3). Significant deviation from standard chemical shift values was observed for the H-α protons of residues Tyr[2], Lys[3], Pro[4], Leu[5], and Gly[6] suggesting some restricted flexibility along the Tyr[2]–Gly[6] sequence. Furthermore, the three bond $^3J_{NH-H-\alpha}$ coupling constant values for residues Leu[5], Gly[6], and Ala[7] are slightly smaller than those measured for the other residues, 5 Hz *versus* 7–8 Hz (Table 3), strengthening the hypothesis of a probable structuring of the Lys[3]–Ala[7] segment. Inter-residues dipolar interactions observed in the ROESY experiment

FIGURE 2. **Structures of the major conformers of peptides in their free (*A*) and mIgA-bound (*B*) forms.** p115 (on *top*), p100c (in the *middle*), and p22 (in the *bottom*) are shown. For each peptide, the backbone of the 10 best calculated structures are superimposed over the residues in β-turn conformation. *B*, the peptides side chains in contact with mIgAs, according to STD experiments, are shown in *green*.

between H-α of Lys[3] and H-δ of Pro[4] indicate that Pro[4] adopts a *trans*-conformation in the major conformer of p100c. In addition to standard sequential interactions, several medium range interactions were also observed between side chain protons of residues Pro[4] to Ala[7] as for example between all protons of Pro[4] and the methyl group of Ala[7] (Fig. 1). Moreover, four long range ROE connectivities were observed between Tyr[2] and His[10] protons, confirming the cyclic nature of the peptide (Fig. 1). ROE derived distances and coupling constants were used as constraints to generate a family of structures for p100c using DYANA. The 10 best structures indicate that the Pro[4]–Pro[7] fragment of p100c is conformationally organized into a type I β-turn (Fig. 2 and Table 2) (61, 62). Because both the cyclic form and Pro[4] can induce this type of conformational behavior, the structural analysis was extended to reduced p100c (data not shown). The type I β-turn remained, suggesting that Pro[4] alone is responsible for its formation, although the cyclic structure might contribute to its stabilization.

Peptide 22 (KRHFLSQRQ)—Available data (Table 4) suggest that p22 is very flexible. Indeed, except for the slight deviation observed for the Ser[6] H-α proton, chemical shifts do not significantly deviate from standard values. Meanwhile, none of the coupling constants of internal residues could be measured because of extensive signals overlaps. Nevertheless, medium range ROE connectivities were observed between side chains protons of residues His[3] and Leu[5] as well as between those of Phe[4] and Ser[6] (Fig. 1). The 10 structures of lowest energy matching those distance constraints show that fragment His[3] to Ser[6] of p22 is organized into a nonclassified β-turn (Table 2), although the peptide N- and C-terminal ends remain quite flexible (Fig. 2). That available chemical shift and coupling constant values do not reflect such an organized conformation in solution suggests a weaker stability of the β-turn.

Ligand Interaction with the Protective mIgAs—Investigation of the molecular pattern of the interactions involved in the peptide- and pentasaccharide-mIgA complexes relied on two complementary methodologies, namely trNOE and STD NMR experiments, whose combination was found to model accurately mAb-ligand interactions (38, 47). Indeed, the former technique provides key information on the conformation of the bound ligand, whereas the latter allows epitope mapping via magnetization transfer from the protein to the residues of the ligand that are in close contact with the protein. To carry out these experiments a few requirements have to be fulfilled as follows: (i) have an important contribution from the bound state to the NOEs, and (ii) have an exchange rate that is fast enough compared with the free ligand longitudinal relaxation. Because here the IC$_{50}$ was the sole information available in terms of binding parameters for the complexes, for each system the best ligand:mIgA ratio was first evaluated from titration experiments according to the method of try and assay.

Binding of DA(E)BC-OMe to mIgA I3 and mIgA C5—Bound pentasaccharide conformation. Independently of the mIgA tested, the best
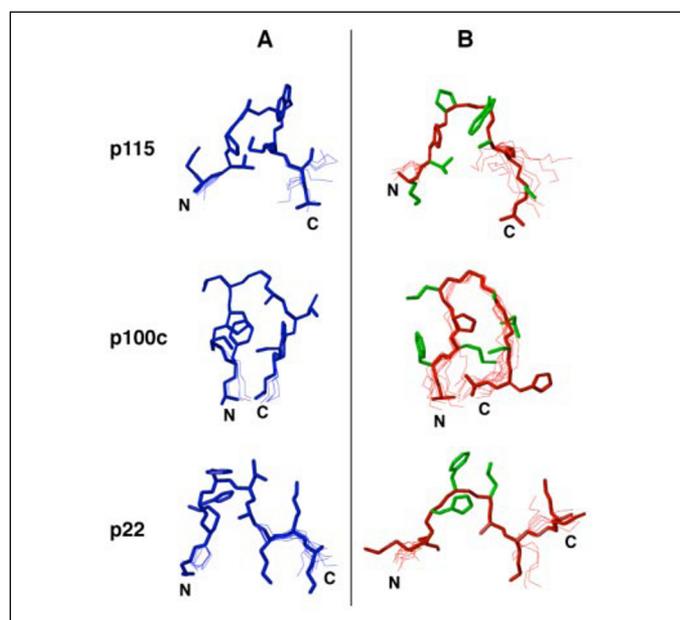
TABLE 2

Characterization of β-turn types of peptides p115, p100c, and p22 free and bound to protective mIgAs

| Peptides | Turns[a] | Position $i + 1$ | | Position $i + 2$ | | β-turn types | |
		ϕ (°)	ψ (°)	ϕ (°)	ψ (°)	Ramachandran nomenclature[b]	Classical nomenclature[c]
p115 free	PPWA	−75.0 ± 0.1	−32.8 ± 0.2	−50.7 ± 0.4	−15.0 ± 0.3	$\beta_p\alpha$	
	PWAR	−50.7 ± 0.4	−15.0 ± 0.3	−46.6 ± 0.1	-20.4 ± 0.2	$\alpha\alpha$	I
p115 mIgA C5	PPWA	−75.0 ± 0.1	140.0 ± 0.4	97.5 ± 0.1	20.7 ± 0.1	$\beta_p\gamma$	II
p100c free	PLGA	−88.8 ± 27.2	−66.6 ± 19.0	−93.3 ± 27.7	6.1 ± 12.1	$\alpha\alpha$	I
p100c mIgA I3	PLGA	−95.0 ± 7.2	64.2 ± 23.0	163.9 ± 23.1	−41.3 ± 13.0	$\beta\gamma$or$\alpha\gamma$	≈II
p22 free	HFLS	159.8 ± 5.8	−30.3 ± 19.4	-153.3 ± 21.1	−18.3 ± 13.1	$\gamma\alpha$	
p22 mIgA I3	HFLS	−121.6 ± 2.3	122.5 ± 0.8	55.7 ± 0.1	76.7 ± 0.5	$\beta_E\gamma$	≈II

[a] Residues in turn conformation.
[b] β-Turn types as defined by Wilmot and Thornton (91).
[c] Richardson classification system (92).

TABLE 3

^{1}H chemical shifts of the *trans*-isomer of p100c in H_2O/D_2O (90/10), pH 5.1 and 298 K

Chemical shifts measured in ppm with an accuracy of ±0.01 ppm are referenced to external 4,4-dimethyl-4-silapentane sodium sulfonate (δ_H 0.00).

Residue	H_N	H_α	H_β	Others
Cys[1]	ND[a]	ND	3.29–3.22	
Tyr[2]	8.87 (7.20)[b]	4.65 / −0,10[c]	3.04–2.91	H-δ 7.12 / H-ε 6.80
Lys[3]	8.05 (8.00)	4.47 / −0,13	1.55	H-γ 1.23 / H-δ 1.63 / H-ε 2.90 / H-ζ 7.45
Pro[4]		4.30 / −0,12	2.23–1.84	H-γ 1.88 / H-δ 3.39
Leu[5]	8.22 (5.30)	4.23 / −0,11	1.61	H-γ 1.61 / H-δ 0.92–0.88
Gly[6]	8.46 (5.40)	4.05–3.74 / −0,09/−0.22		
Ala[7]	8.02 (5.40)	4.31 / −0,01	1.38	
Leu[8]	8.32 (7.20)	4.37 / 0,03	1.69	H-γ 1.62 / H-δ 0.92–0.85
Thr[9]	7.69 (7.80)	4.30 / −0,05	4.17	H-γ 1.15
His[10]	8.30 (7.80)	4.38 / −0,35	3.36	H-ε1 8.58 / H-δ2 7.31
Cys[11]	8.49 (7.40)	4.51 / −0,20	3.28–3.05	

[a] ND indicates not determined.

[b] Data in parentheses are $^3J_{HN,H\alpha}$ coupling constants (in Hz ± 0.2 Hz) measured from the one-dimensional spectrum.

[c] Data in italics are the difference between the Hα chemical shifts of the residues of the peptide and those of the same residues in nonstructured peptides GG*X*AGG or GG*X*PGG (90).

TABLE 4

^{1}H chemical shifts of the *trans*-isomer of p22 in H_2O/D_2O (90/10), pH 5.1 and 298 K

Chemical shifts measured in ppm with an accuracy of ±0.01 ppm are referenced to external 4,4-dimethyl-4-silapentane sodium sulfonate (δ_H 0.00).

Residue	H_N	H_α	H_β	Others
Lys[1]	ND[a]	3.88 / −0,41	1.80	H-γ 1.36 / H-δ 1.67 / H-ε 2.96 / H-ζ ND
Arg[2]	ND	4.28 / −0,06	1.68	H-γ 1.52 / H-δ 3.14 / H-η ND
His[3]	ND	4.76 / −0,03	3.18–3.00	H-ε1 7.86 / H-δ2 6.98
Phe[4]	8.22 (7.20)	4.59 / −0,03	3.09–2.97	H-δ 7.20 / H-ε 7.29 / H-ζ 7.33
Leu[5]	8.33 (ND)	4.32 / −0,02	1.57	H-γ 1.50 / H-δ 0.89–0.84
Ser[6]	8.22 (ND) (6.70)	4.38 / −0,09	3.85	
Gln[7]	8.35 (ND)	4.35 / 0,01	2.11–1.96	H-γ 2.34 / H-δ 6.82–7.53
Arg[8]	8.33 (ND)	4.32 / −0,02	1.86–1.74	H-γ 1.62 / H-δ 3.18 / H-η ND
Gln[9]	8.04 (7.70)	4.15 / −0,19	2.09–1.90	H-γ 2.28 / H-δ 6.78–7.50

[a] ND indicates not determined.

[b] Data in italics are the difference between the Hα chemical shifts of the residues of the peptide and those of the same residues in nonstructured peptides GG*X*AGG or GG*X*PGG (90).

[c] Data in parentheses are $^3J_{HN,H\alpha}$ coupling constants (in Hz ± 0.2 Hz) measured from the one-dimensional spectrum.

DA(E)BC-OMe:mIgA ratio to observe trNOEs was shown to be 20:1 in binding sites. Because the highest attainable mIgA concentration was 3.75 μM, a 0.3 mM concentration of DA(E)BC-OMe was used to fulfill the 20:1 ratio requirement. Because NOE intensities depend, among other parameters, on the correlation time for reorientation and therefore on temperature, the later parameter was optimized so that $\omega\tau_c$ equals 1 for the free pentasaccharide, thus allowing us to distinguish NOE from trNOE connectivities. Indeed, the NOESY spectrum of the free pentasaccharide at 30 °C displayed only few positive and weak NOE connectivities characteristic of small molecules, whereas negative NOE connectivities were observed in the trNOESY spectrum of DA(E)BC-OMe when interacting with either mIgA C5 or mIgA I3. Because these effects did not result from the increased solution viscosity as probed by recording NOESY spectra of the pentasaccharide in the presence of BSA at the same w/v concentration (37), it was assumed that they corresponded to trNOE connectivities for the mIgA-bound DA(E)BC-OMe.

trNOESY spectra obtained with several mixing times, ranging from 100 to 400 ms, allowed us to trace the build-up curves (trNOEs intensities *versus* τ_m) from which the distance information was extracted. In addition, inter-residue ^1H–^1H distances were also calculated from a trROESY spectrum obtained with a mixing time of 400 ms to take spin diffusion into account, if any. Comparison of these distances with those measured for unbound DA(E)BC-OMe (33) suggested that the pentasaccharide conformation was not significantly modified upon binding to the mIgAs (Table 5).

Epitope Characterization—The key elements involved in DA(E)BC-OMe binding to the mIgAs were then characterized based on STD experiments. As for the trNOE experiments, an oligosaccharide to mAb ratio of 20:1 in binding site was used. To decrease the exchange rate, the temperature was set at 15 °C. The one-dimensional STD spectrum of DA(E)BC-OMe interacting with mIgA C5 shows that protons H1 and H2 and H6 (methyl group) of rhamnoses A and B, as well as all protons belonging to glucose (E), are in close contact with the mIgA C5-binding

site (Fig. 3). Indeed, these interacting protons were fully identified in the corresponding two-dimensional STD-TOCSY spectrum (Fig. 4). Similar results were obtained for DA(E)BC-OMe binding to the mIgA I3 (data not shown). Furthermore, protons from the glucose (E) and the methyl group of residue B give the strongest signal enhancements, suggesting that they are in closest contact with both mIgAs (Fig. 5) and play a crucial role in the oligosaccharide-mAb interaction.

Binding of the Peptide Mimics to mIgAs—Based on available IC_{50} values, analysis was run on the p115-mIgA C5, p100c-mIgA I3, p22-mIgA C5, and p22-mIgA I3 complexes.

Interaction of Peptide 115 (KVPPWARTA) with mIgA C5—trNOE experiments recorded for the p115-mIgA C5 complex (see supplemental Fig. 4S) showed new NOE connectivities when compared with those observed for the free peptide. These additional cross-peaks, such as those observed between residues Trp[5] and Ala[6], were clearly identified as representative of the p115-bound form. Interestingly, most of the NOE connectivities involving amide protons of the free p115 were no longer observed in bound p115 with the exception of the Trp[5], Ala[6] amide proton connectivity (see supplemental Fig. 1S). The pH increase from 5 in the free peptide to 6.5 in the peptide:mIgA solution might account for such experimental observations since amide protons exchange faster at higher pH. Nevertheless, the medium range NOE connectivities observed between the side chain proton of residues Val[2] and Pro[3], and the CH_3-β of Ala[6] remained (see supplemental Fig. 1S). Distance constraints derived from trNOE intensities were used to establish the conformation of p115 when bound to mIgA C5. Superimposition of the 10 lowest energy backbone conformations of free p115 to those of mAb-bound p115 showed that only the turn involving residues Pro[3] to Ala[6], observed in the free form, is maintained in the bound form. Based on $C\text{-}\alpha_i$–$C\text{-}\alpha_{i+3}$ distances as well as on Φ and Ψ angle values (Table 2) the type I β-turn observed between residues Pro[4] and Arg[7] for the free peptide is no longer present. Whereas in the free form fragment

TABLE 5

^{1}H-^{1}H inter-residue distances (Å) extracted from dipolar interactions observed in ROESY and NOESY spectra of DA(E)BC-OMe pentasaccharide free and in interaction with mIgA C5 and mIgA I3

The two values correspond to distances extracted from ROESY (400 ms) (left) and NOESY (right), respectively (accuracy, ±10%). ND indicates not determined.

Proton pairs[a]	DA(E)BC-OMe	DA(E)BC-OMe/IgA C5	DA(E)BC-OMe/IgA I3
A-1/B-1	3.3/ND	ND/3.0	ND/2.9
A-1/B-2	2.2/ND	ND/2.4	2.1/2.2
A-5/B-1	2.4/2.5	ND/2.7	2.4/2.5
A-6/B-1	3.4/3.4	ND/3.2	ND/3.2
B-1/C-3	2.3/2.3	ND/2.3	2.3/2.2
B-2/E-1	2.3/ND	ND/2.5	2.2/2.3
B-3/E-1	2.5/2.5	ND/3.2	2.8/2.8
B-3/E-5	3.3/3.2	ND/2.7	ND/2.7
B-6/C-2	3.6/3.5	ND	ND/3.5

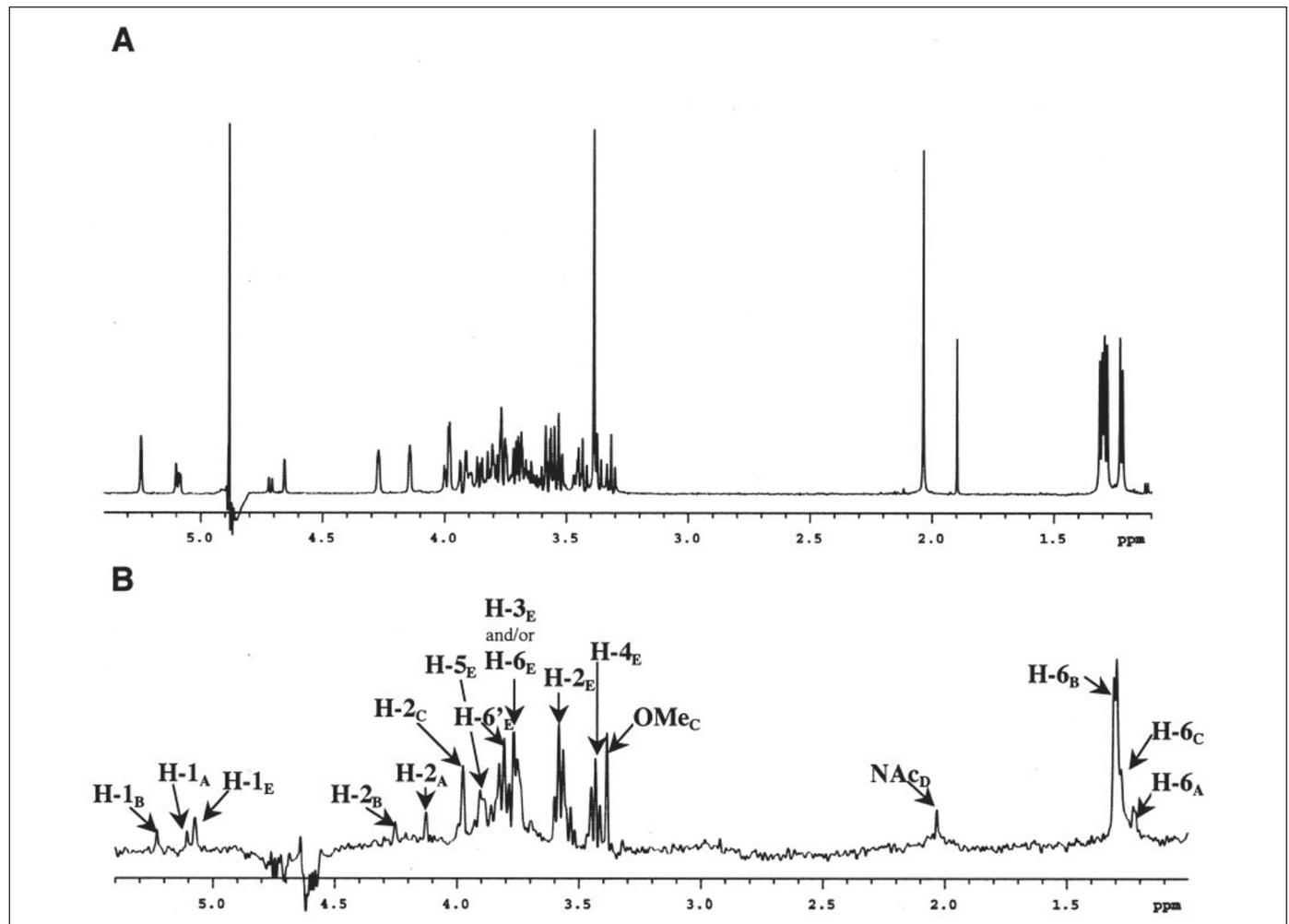[a] A-1 corresponds to proton 1 of rhamnose A.

FIGURE 3. **mAb binding epitope of the pentasaccharide DA(E)BC-OMe.** *A,* one-dimensional ^{1}H reference spectrum of pentasaccharide DA(E)BC-OMe in the presence of mIgA C5 (20:1 ratio in site). *B,* one-dimensional STD-NMR of DA(E)BC-OMe in the presence of mIgA C5 with selective saturation of antibody resonances at 0.3 ppm. Protons of DA(E)BC-OMe affected by the selective saturation of mIgA C5 and so in contact with the mAb are labeled.

Pro[3]–Ala[6] adopts a nonclassified type of β-turn, in the bound form a well defined type II β-turn is clearly present (61, 62) (Fig. 2 and Table 2).

STD experiments (Fig. 6), run under the experimental conditions used for trNOE experiments, showed that the p115 protons in close contact with mIgA C5 are the side chain protons of Lys[1] and Pro[4], all the methyl groups thus implicating Val[2], Ala[6], and Ala[9], and all protons of the Trp[5] aromatic ring. Clearly, in addition to side interactions involving the N- and C-terminal ends, major contacts involve residues from the Pro[4]– Ala[6] segment, suggesting that the structured Pro[3]–Ala[6] type II

β-turn is crucial for p115:mIgA C5 recognition. It is worth noting that the major form of p115 was that recognized by mIgA C5.

Interaction of Peptide p100c (CYKPLGALTHC) with mIgA I3—As compared with data corresponding to the free form, the trNOESY spectrum of p100c in interaction with mIgA I3 displayed new data specific for the bound form. These include new sequential NOEs such as those observed between Lys[3] and Pro[4] or between Pro[4] and Leu[5], whereas sequential NOEs between Ala[7] and Leu[8], or between Leu[8] and Thr[9], were no longer visible. However, medium range NOE connectivities

FIGURE 4. **The branched glucose residue E of the pentasaccharide DA(E)BC-OMe constitutes a key element in mAb recognition.** *A,* two-dimensional STD-TOCSY of DA(E)BC-OMe in the presence of mIgA C5 (20:1 ratio in site) with selective saturation of antibody resonances at 0.3 ppm. *B,* a zooming of the two-dimensional STD-TOCSY in the 3.4–4 ppm region emphasizing the glucose E proton connectivities.
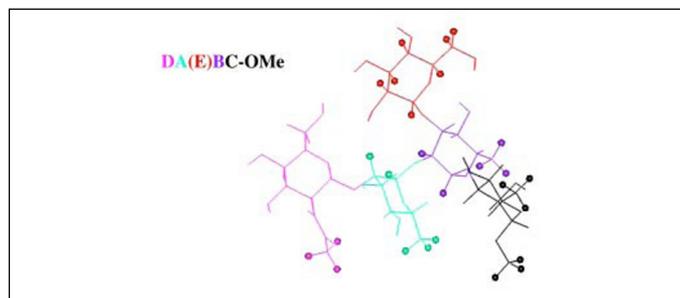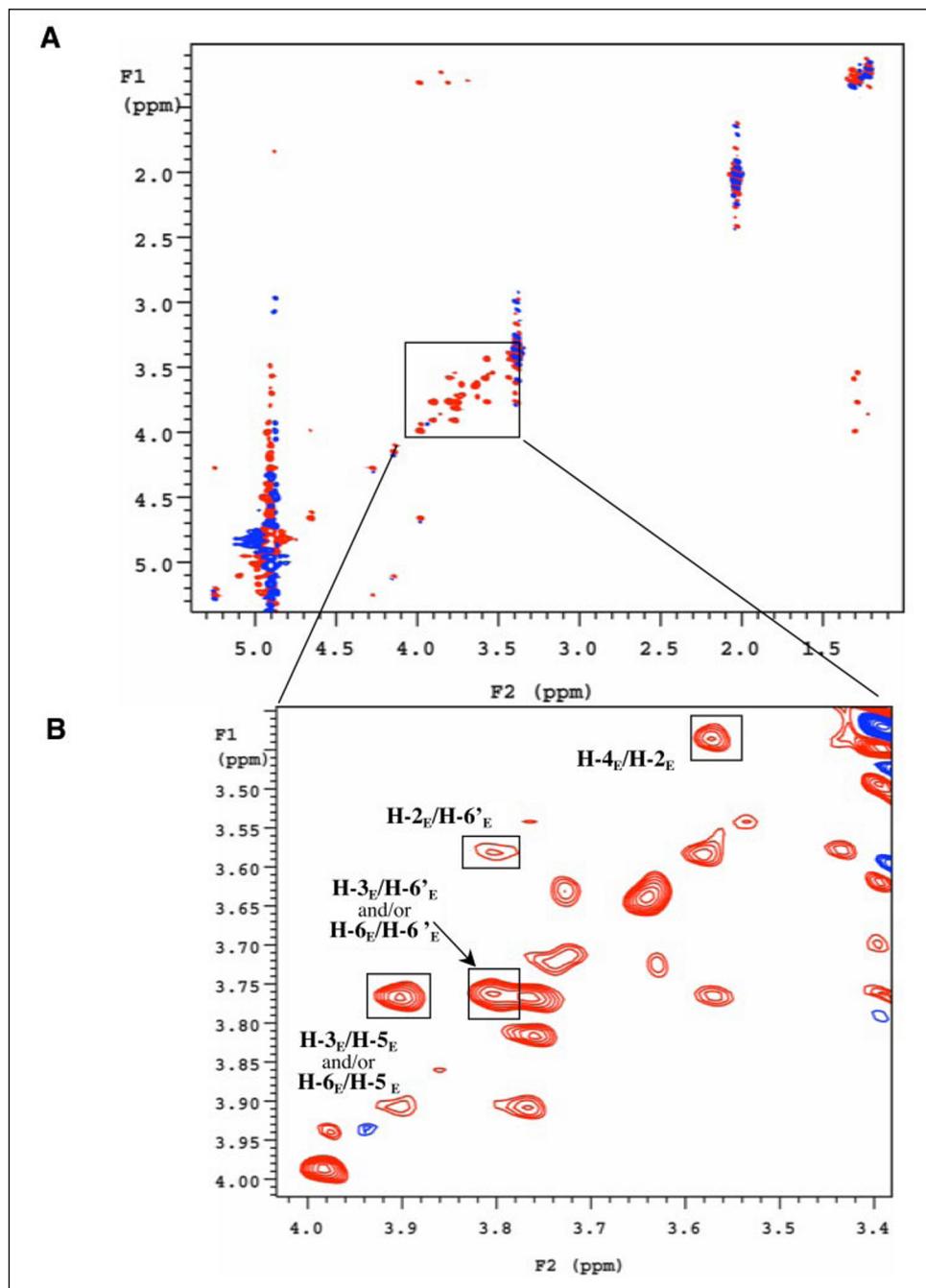

FIGURE 5. **Structure of the pentasaccharide DA(E)BC-OMe.** The representation of a lowest energy conformation of DA(E)BC-OMe as determined with the CICADA method and in agreement with NMR data (33). The *small spheres* indicate the protons that are in contact with the protective mAbs, mIgA C5, and mIgA I3, in agreement with the STD-NMR experiments.

observed between Pro[4] and Ala[7] in the free form remained. In addition, medium range interactions specific to the bound form were observed, such as those involving side chain protons of Tyr[2] and Leu[5], Lys[3] and Leu[8], as well as Tyr[2] and His[10] (see supplemental Fig. 2S). Superimposition of the backbone (Pro[4] to Ala[7] fragment) of the 10 lowest energy conformations of free and mIgA I3-bound p100c matching the distance constraints showed that, as observed for p115, the turn observed in the free form was maintained in the bound form. Furthermore, data pointed to a switch from a type I β-turn in the free form to a type II β-turn in the bound form (Table 2) (61, 62). Additional significant rearrangements were observed for the rest of the backbone (Fig. 2).

More detailed epitope identification was derived from the one-dimensional STD experiment. All methyl group protons of p100c, thus involving residues Leu[5], Ala[7], and Leu[8] as well as the Tyr[2] side chain
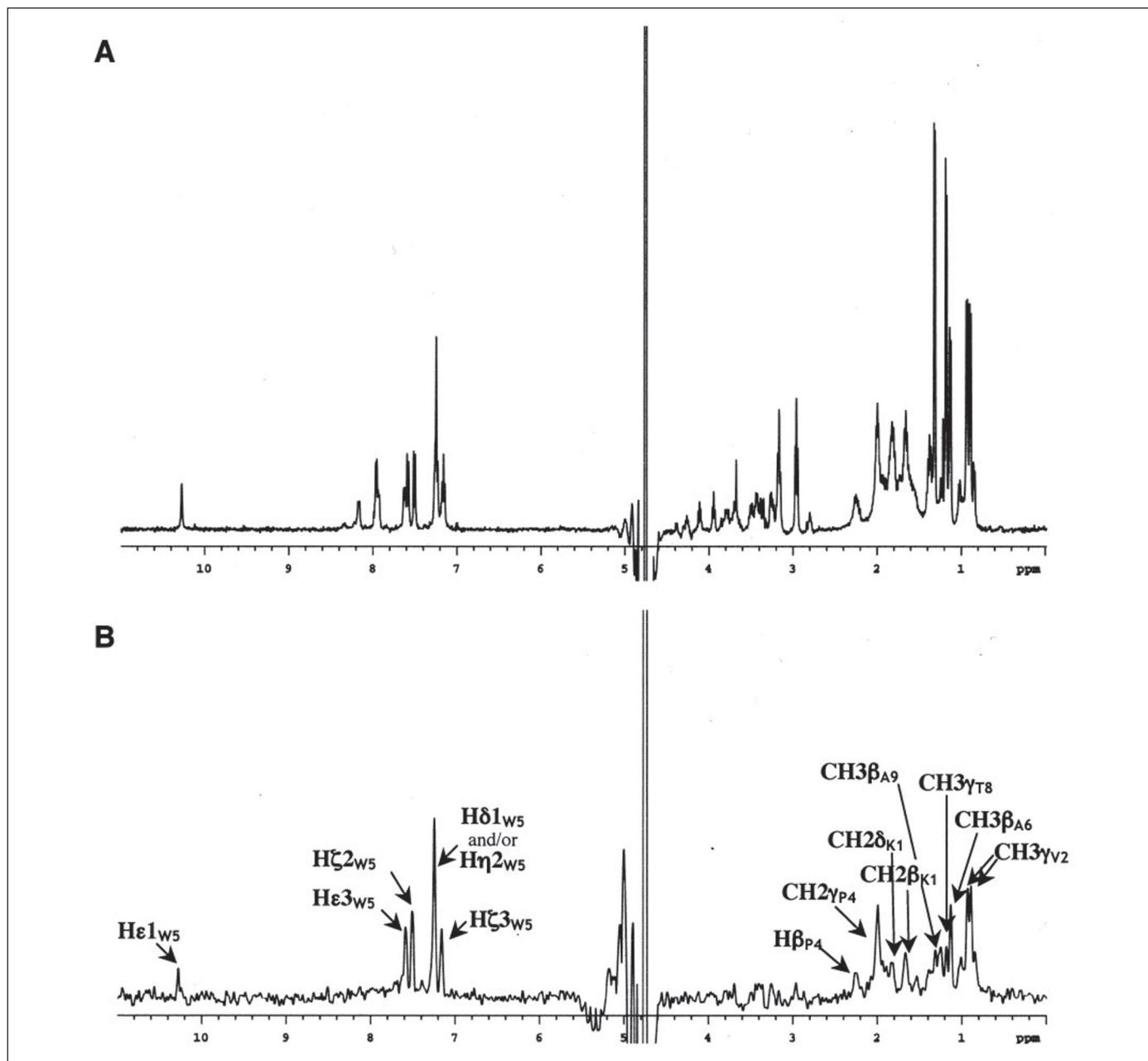
FIGURE 6. **mAb binding epitope of the peptide p115.** *A,* one-dimensional reference spectrum of p115 in the presence of mIgA C5 (20:1 ratio in binding site). *B,* one-dimensional STD-NMR of p115 in presence of mIgA C5 with selective saturation of mAb at 0.3 ppm. Protons of p115 affected by the selective saturation and so in interaction with mIgA C5 are labeled.

protons and the Lys[3] CH2-γ protons, were in contact with the mIgA I3 (Fig. 7). Within the turn, only Leu[5] and Ala[7] methyl groups contacted the mAb. Similarly to p115, the methyl groups of the hydrophobic residues and the aromatic residue of p100c were involved in the interaction with the mIgA I3.

Interaction of Peptide p22 (KRHFLSQRQ) with mIgA I3 and mIgA C5— Comparison with the spectrum of the free peptide shows that the trNOE connectivities observed when p22 is bound to mIgA I3 differ for medium range interactions. Indeed, dipolar interactions observed between Phe[4] and Ser[6] in free p22 disappeared to the benefit of new interactions between His[3] and Ser[6] in the bound form. However, dipolar interactions between His[3] and Leu[5] were observed both in the free and the bound forms (see supplemental Fig. 3S). Comparison of the lowest energy conformations adopted by p22 in the free and bound forms showed that the nonclassified β-turn

involving the His[3]–Ser[6] segment in the free form changed to a type II β-turn in the bound form, as observed for p115 and p100c. Additional rearrangements were observed for the rest of the backbone (Fig. 2). trNOE experiments for p22 bound to the mIgA C5 were unsuccessful because sparse negative NOEs were observed (data not shown). The high affinity of mIgA C5 (IC$_{50}$ of 0.03 μM), most probably associated with an equilibrium constant for dissociation (K_d) below 10^{-6} M and thus not compatible with trNOE observations ($10^{-3} > K_d > 10^{-6}$ M), might be responsible for this effect. Despite this drawback, epitope mapping by STD experiments was successfully undertaken as the lower limit for exchange was less stringent in terms of K_d (10^{-8} M). Epitope identification for p22 bound to mIgA I3 and mIgA C5, respectively, was obtained from the one-dimensional STD experiments (Fig. 8). Whether mIgA I3 or IgA C5 was concerned, p22 residues in direct contact with the mAbs were identical. They included the His[3] imid-
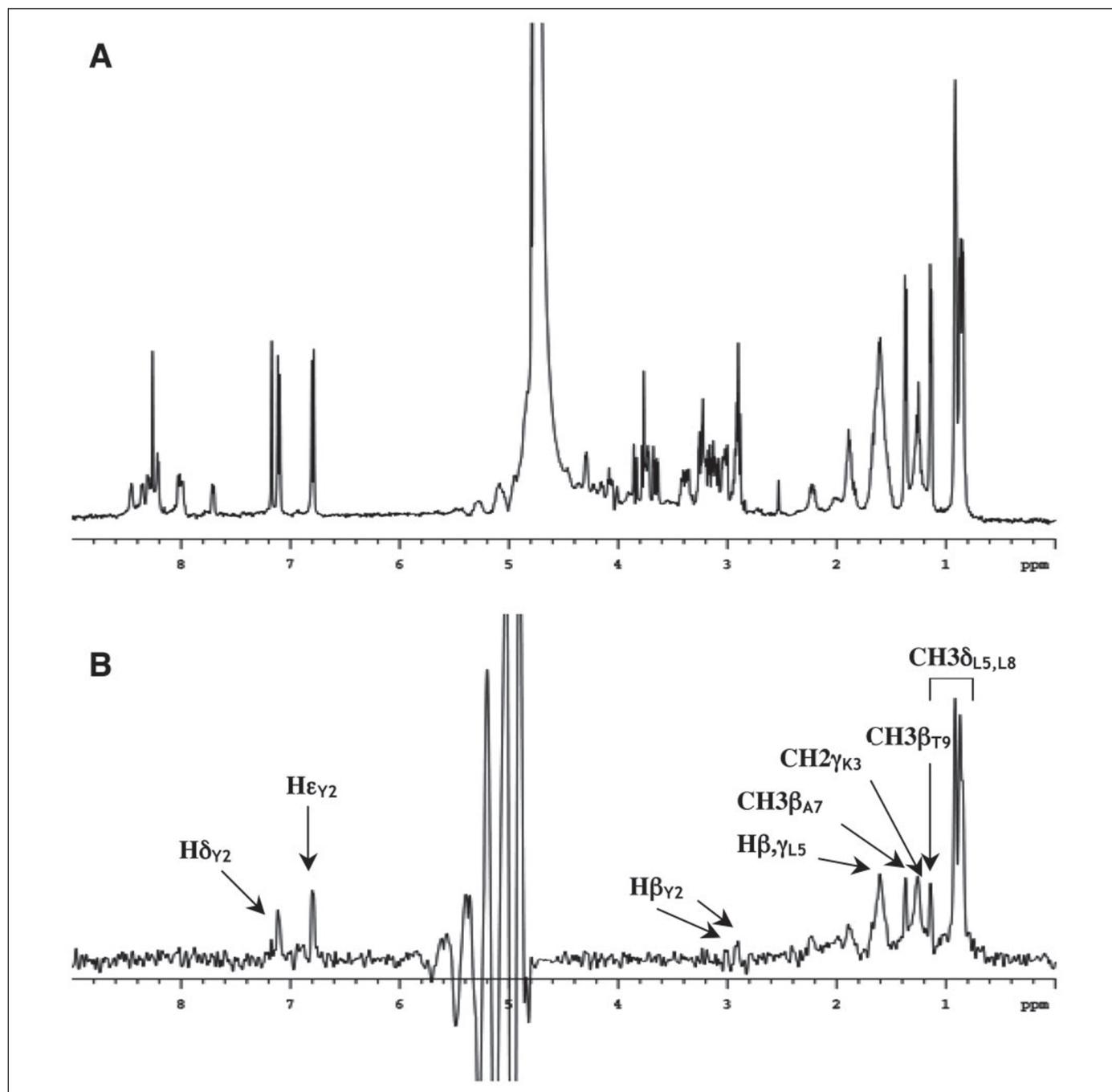
FIGURE 7. **mAb binding epitope of the peptide p100c.** *A,* one-dimensional reference spectrum of p100c in presence of mIgA I3 (20:1 ratio in binding site). *B,* one-dimensional STD-NMR of p100c in presence of mIgA I3 with selective saturation of mAb resonances at 0.3 ppm. Protons of p100c affected by the selective saturation and so in interaction with mIgA I3 are labeled.

azole protons, Phe[4] aromatic protons, as well as Leu[5] methyl protons, all corresponding to amino acids taking part in the turn observed in free p22. Although the conformation of mIgA C5-bound p22 remained undisclosed, available data suggest that the nonclassified turn naturally adopted by p22 contributed to both mIgA I3 and mIgA C5 recognition.

Modeling of the Fab Domain of mIgA I3—A blast search in the Protein Data Bank (55) allowed us to identify three mAb chains with high sequence similarity to either the VL or the VH chain of mIgA I3. Sequence alignments are displayed in Fig. 9 together with Protein Data Bank code for the structures of interest that include anti-RNA mAb (code 1MRD) (63), the anti-DNA mAb (code 1CBV) (64), the catalytic mAb (code 1A4J) (65), anti-influenza neuraminidase (code 1NCA) (66), and anti-cholera toxin mAb

(code 1TET) (67). Each chain was built by homology modeling using the standard procedure of the composer program (56). The murine Fab fragment with Diels-Alder catalytic properties (65) displayed high similarity for both chains and was used as a template for assembling the two chains. As a general feature for mAbs, the H3 loop of CRD is known as the most variable one. Among the structures with high homology, the H3 loop of the anti-cholera toxin Fab (67) was selected as a template because it displays the same number of amino acids as the target. After optimization of the side chain conformation, the binding site of mIgA I3 appeared to have a distinct "groove" character located between the variable loops with a deep central pocket. The sides of the groove were flanked by the CDRs, mostly H2 and H3 of the heavy chain and L1 in the light chain.
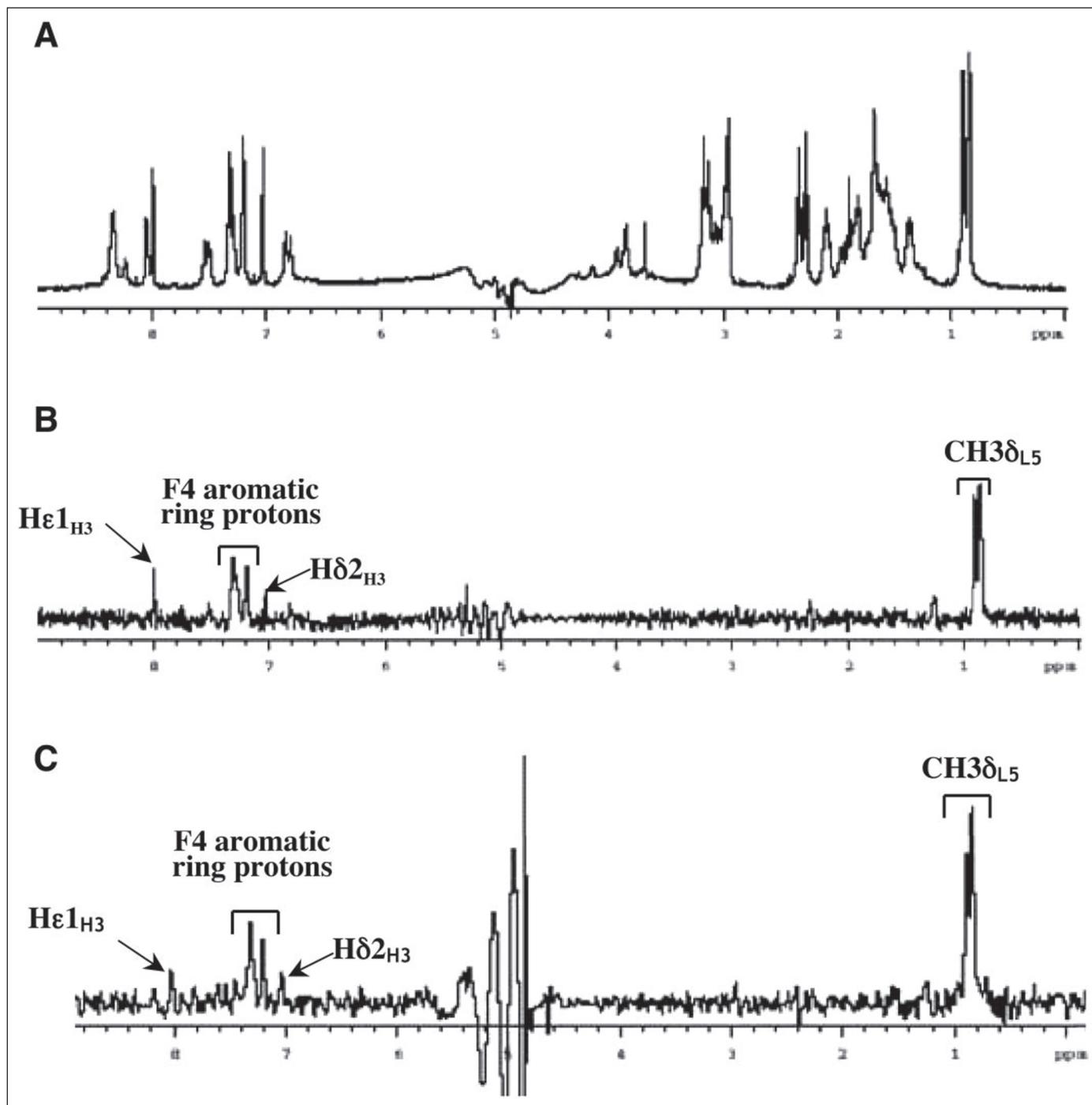
FIGURE 8. **mAb binding epitope of the peptide p22.** *A,* one-dimensional reference spectrum of p22 in presence of mIgA I5 (20:1 ratio in binding site). *B,* one-dimensional STD-NMR of p22 in presence of mIgA I3. *C,* one-dimensional STD-NMR of p22 in presence of mIgA C5. The selective saturation of mAb resonances was done at 0.3 ppm. Protons of p22 affected by the selective saturation and so in contact with the mAbs are labeled.

Docking of Oligosaccharides and Modeling of Complexes with mIgA I3—Previous studies identified two different helical conformations of *S. flexneri* 5a O-SP as being the most stable ones in solution (33). Both can be described as right-handed 3-fold helices, but one is more extended (E) than the other (O) with helical repeats of 23.2 and 19.4 Å, respectively. The nonasaccharide BCDA(E)BCDA was selected for docking studies as the largest O-SP fragment that can be treated as a flexible ligand. When the nonasaccharide BCDA(E)BCDA fixed in both conformations is docked into the Fab-binding site, four solutions can be identified, two for the E conformation and two for the O one. In both cases, the nonasaccharide can

fit either with a parallel orientation to the binding site groove or with a perpendicular one. In any case, the branched α-D-glucopyranose residue E is deeply buried into the central pocket of the groove. In all of the four solutions, the mAb features involved in carbohydrate recognition are the three loops from the heavy chain and the L1 and L3 loops from the light chain. The variable loop H3 plays the major role, with its two Asp residues (Asp[91] and Asp[92]) involved in recognition for most binding modes.

When the nonasaccharide-bound conformations were propagated into polysaccharide structures comprising four repeating units, only two docking modes appeared to be stable with additional contacts cre-
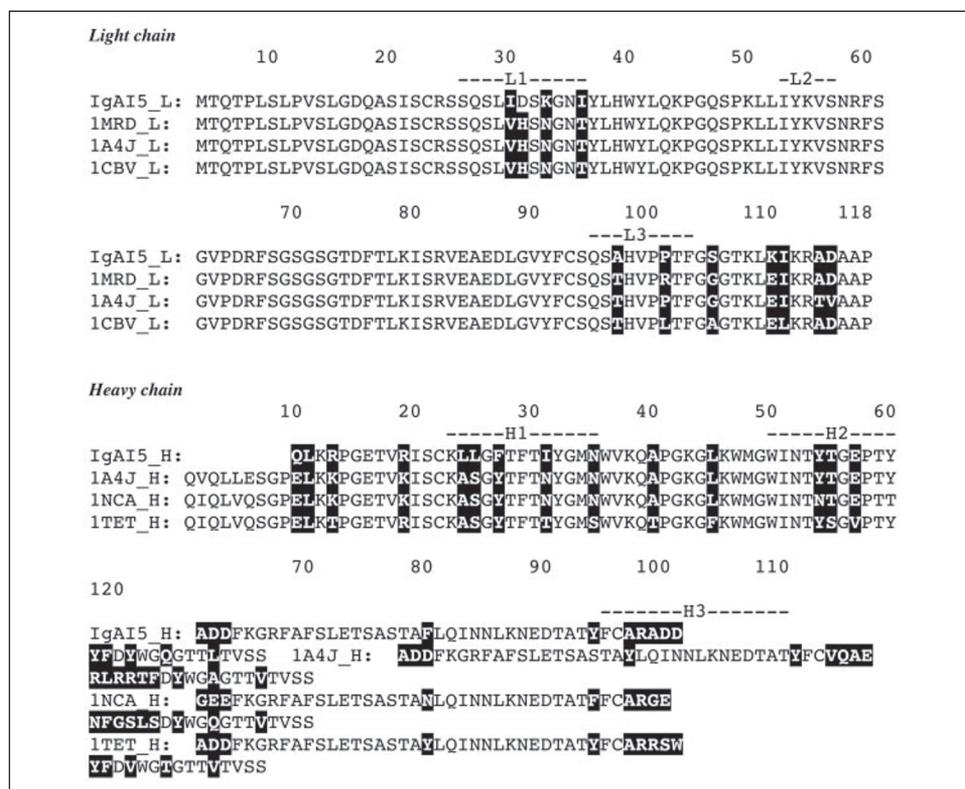
FIGURE 9. **Alignment of mIgA I3 sequence with related sequences taken from the Protein Data Bank.** Sequence differences are highlighted by displaying amino acid code using *white letter on black background*.

ated on both sides of the binding site. In each case, this ability corresponded to the parallel arrangement of BCDA(E)BCDA. Therefore, only these two solutions, *i.e.* docking of E and O conformations in parallel mode, were considered as possible mimics of O-SP binding to mIgA I3. The two possible docking modes of BCDA(E)BCDA and the polysaccharide of DP4 are displayed in Fig. 10 (*A–D*) and the contacts of interest are listed in Table 6. For both conformations of each ligand, the central trisaccharide A(E)B makes most of the binding contribution, and the additional contacts established by the GlcNAc (D) residue are minor.

Docking of Peptide Mimics—Docking of peptides to mAbs was performed on one example in order to rationalize the protective effect. The cyclic peptide p100c is conformationally constrained and was therefore selected for the modeling studies with the mAb that displays the highest affinity, *i.e.* mIgA I3. For the two lowest energy docking solutions, the p100C conformation displayed good shape complementarity with the binding site central pocket of mIgA I3. In the first solution, a strong interaction (three H-bonds and two salt bridges) appeared between the peptide and the mAb, mainly located on CDRH3 domain involving Asp[91] and Asp[92] (Table 6). The second docking solution led to identical main interactions between p100c and CDRH3 (Table 6). In both cases, the Leu[5]–Gly[6]–Ala[7] motif of p100c, seen as constrained by NMR, was driven into the central pocket (van der Waals interactions). Both docking modes allowed for a strong interaction between the Lys[3] of the peptide and the protein Asp[92]. Nevertheless, the Tyr[2] residue of the peptide was buried in the second solution and established strong van der Waals contacts with the aromatic side chain of Trp[41] and Phe[94] of mIgA I3. Therefore, this model displayed in Fig. 10 (*E* and *F*) was that in best agreement with NMR data.

DISCUSSION

As a novel strategy to improve vaccine design, molecular mimicry has gained a growing interest in the recent past. For mimicry of polysaccharides, the mimics can be of the same molecular class as the natural antigen, *i.e.* oligosaccharides, or different, as for instance the peptide mimics. The nature of peptide carbohydrate mimicry has not yet been deciphered, and detailed structural studies of both oligosaccharide-mAb complexes and carbohydrate-mimicking peptides-mAb complexes are still needed to expand the thus far limited structural data base available in the series. Peptide-carbohydrate mimicry is either structural, functional, or both. Structural mimicry resides in mimicry of specific chemical groups of the carbohydrate by chemical groups of the peptide, thus both ligands contact the same residues in the mAb-binding site (68). Mimicry is termed functional when the mimic differs structurally from the natural antigen. Both the antigen and the mimic cross-react specifically with the mAb used for selection, although the protein residues involved in recognition differ (17, 21, 69).

Here, by aiming at designing new vaccine strategies against *Shigella* infection, we developed synthetic mimics, carbohydrates and peptides, of *S. flexneri* 5a O-SP. Previous NMR and molecular modeling studies from our laboratory have shown that, among the four possible frame-shifted pentasaccharides representative of the O-SP, DA(E)BC-OMe best mimics the conformational features of *S. flexneri* 5a O-SP (33). More importantly, the trNOE data reported here indicate that the conformation of DA(E)BC-OMe when bound to O-SP-specific mIgA I3 and mIg C5 does not differ from its conformation when free in solution. Noteworthy, selection of free solution conformers often predominates in mAb-carbohydrate recognition processes (70). However, it is not always so as exemplified with mAb Se155-4 binding to a trisaccharide antigenic determinant of the *Salmonella paratyphi* B branched O-SP (71).

Another interesting example of such induced conformational change is the mAb SYA/J6 binding to the pentasaccharide ABCDA′ fragment of the linear O-SP defining *S. flexneri* serotype Y (72). Modeling of the linear heteropolysaccharide has shown that it is structured into a left-handled helical chain of three ABCD repeating units (73, 74). Most interestingly, extension of the modeling study to *S. flexneri* 5a O-SP
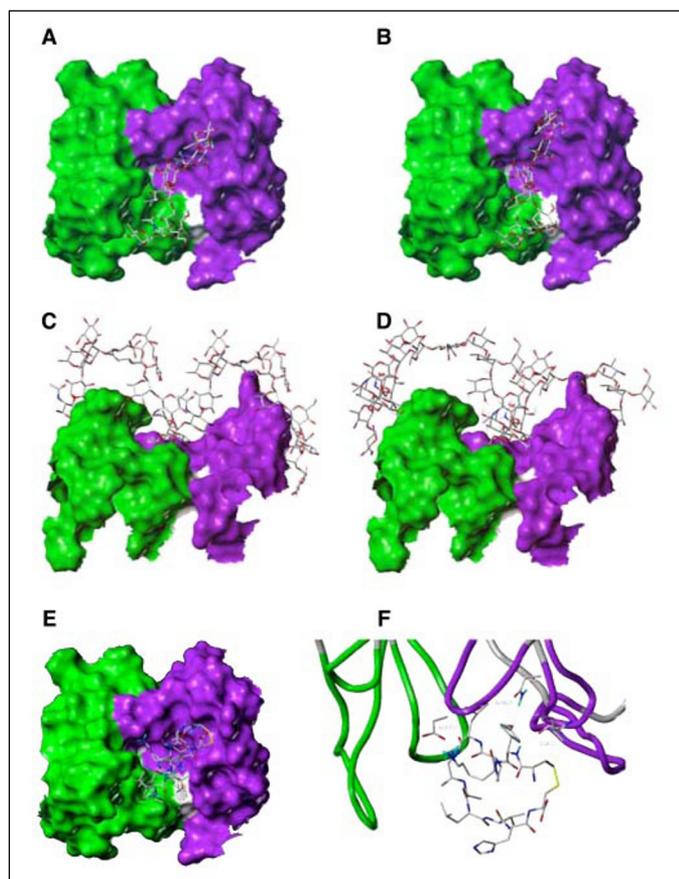
FIGURE 10. **Graphical representation of the different models of antibody mIgA I3 (light chain in *green* and heavy chain in *violet*) with docked oligosaccharide and cyclic peptide p100c.** *A* and *B,* two possible docking modes for nonasaccharide in mIgA I3. *C* and *D,* corresponding interaction with the polysaccharide (four repeating units) after propagation of the nonasaccharide conformation along the 20-residue chain. *E* and *F,* two different views of the docking mode of p100c in mIgA I3-binding site displaying the best agreement with NMR data.

TABLE 6

Contact between ligand and antibody in the different model for docking oligosaccharide and cyclic peptide p100c

Ligand atom	Protein atom	Aβ chain
Oligosaccharide model 1 (extended)		
D:GlcNAc.O4-H	Ile^{22}.O	H1
D:GlcNAc.O6-H	Ala^{90}.O	H3
D:GlcNAc.O6	Gly^{24}.NH	H1
A:Rha.O3-H	Asp^{92}.COO$^-$	H3
A:Rha.O4	Lys^{30}.NH3$^+$	L1
E:Glc.O3-H	Asp^{91}.COO$^-$	H3
E:Glc.O3	Tyr^{93}.NH	H3
B:Rha.O4-H	Ser^{93}.O	L3
Oligosaccharide model 2 (extended)		
D:GlcNAc.O6	Gly^{24}.NH	H1
E:Glc.O$_2$-H	Asp^{91}.O	H3
E:Glc.O3-H	Asp^{91}.O	H3
E:Glc.O3	Tyr^{93}.NH	H3
B:Rha.O4-H	Ser^{93}.O	L3
A:RhaO4	Ser^{29}.OH	L1
Peptide p100c model 1		
H-bonds		
Lys^3.NH3$^+$	Asp^{91}.COO$^-$	H3
Lys^3.NH3$^+$	Asp^{92}.COO$^-$	H3
Leu^5.O	Gly^{24}.NH	H1
His^{10}.NH$^+$	Asp^{28}.COO$^-$	L3
His^{10}.NH$^+$	Ser^{29}.OH	L3
Hydrophobic interactions		
Pro^4	Trp^{41}	L2
Ala^7	Trp^{41}	L2
Peptide p100c model 2		
H-bonds		
Tyr^2.NH	Ile^{22}.O	H1
Tyr^2.OH	Asn^{26}.NH$_2$	H1
Lys^3.NH3$^+$	Asp^{92}.COO$^-$	H3
Hydrophobic interactions		
Tyr^2	Trp^{41}	L2
Pro^4	Trp^{41}	L2
Pro^4	Phe^{94}	H3
Pro^4	Pro^{98}	H3

suggested that residue E, which is associated with serotype specificity, crucially impacts the overall O-SP conformation. In fact, the branched heteropolysaccharide, whose repeating unit (I) bears the E side chains, behaves as a right-handed 3-fold helix with residue E protruding outwardly (33). Along this line, the interaction of DA(E)BC-OMe with the serotype-specific mIgAs is mainly driven by the branched E residue as evidenced by the large number of E-specific signals enhanced in the STD spectra of the pentasaccharide in complex with mIgA I3. Furthermore, NMR experiments showed that all rhamnose methyl groups are also in close contact with the mAb, with the methyl group of rhamnose B on which E is branched being the major contributor. The *N*-acetyl group of residue D gives only weak contacts with the mIgA protons, indicating that it probably lies at the surface of the mAbs. These data are supported by the inhibition ELISA results showing that all frame-shifted tri-, tetra-, and pentasaccharides, bearing A(E)B-branched trisaccharide characteristic of *S. flexneri* 5a serotype, are recognized by a protective serotype 5a-specific mIgG (33). Further insights on the central role played by the branched α-D-glucopyranosyl residue E in mAb recognition derives from docking of the nonasaccharide BCDA(E)BCDA and fragments of the O-SP comprising four repeating units in the mIgA I3 Fab-binding site. The latter appears to have a distinct groove character with a deep central pocket, a type of binding site often encountered for mAbs binding internal polysaccharide sequences (75). Most interestingly, this finding is identical to that observed for Strep 9, a mouse mAb of the IgG3 subclass directed against the cell wall polysaccharide of

group A *Streptococcus* (76) made of repeats comprising a branched β-*N*-acetyl-D-glucosamine residue linked to a linear di-rhamnopyranosyl backbone. As found earlier, sides of the mIgA I3 groove are flanked by CDR2 of the heavy chain and CDR1 of the light chain. Moreover, aromatic residues such as Tyr^{45} of the heavy chain and Tyr^{34} of the light chain define the pocket region, pointing once more to the importance of such amino acids in carbohydrate recognition (77, 78). Indeed, whatever the orientation of nonasaccharide BCDA(E)BCDA, parallel or perpendicular relative to the groove binding site, the glucose residue E was always deeply buried in the central pocket of the groove and was poorly accessible to solvent. Most interestingly, relying on molecular modeling only, a heptasaccharide related to *Brucella abortus* O-SP exemplifies another O-SP-mAb interaction for which the mAb-binding site identified as a groove bearing a pocket in its center could also accommodate two binding modes of an O-SP fragment (79). As shown here, docking of *S. flexneri* 5a O-SP large fragments in the mIgA I3-binding site pointed to only one possible binding mode of the O-SP, namely the parallel mode, independently of the length of the helical repeat taken into account. Thus, in addition to the branched glucopyranosyl residue E behaving as an anchor and to the trisaccharide A(E)B providing the critical epitope exposed on the O-SP, chain elongation also takes part in O-SP:mIgA recognition, highlighting the essential contribution of some kind of conformational epitope or presentation in an extended surface. However, we are aware that small changes at the $V_L:V_H$ interface of the mAb may result in significant alteration of the binding mode, which cannot be predicted at this stage (80). Thus, data provided here are only meant to provide a model of *S. flexneri* 5a O-SP binding to a homologous protective mIgA, which needs to be further assessed based on crystallographic data.

Peptide Mimics of *S. flexneri* 5a Polysaccharide Antigen

Peptides cross-reacting with *S. flexneri* 5a O-SP have been identified by screening phage-displayed peptide libraries with protective mIgA C5 and mIgA I3 (28). Nonconstrained and constrained peptide libraries were screened. Indeed, it is expected that constraining a peptide limits its flexibility and therefore may improve its affinity for mAb binding, and consequently, may allow the selection of better mimics of the natural antigen (81). All selected peptides, whether mimotopes or mimics only, exhibited an IC_{50} value ranging from micromolar to submicromolar (this work and Footnote 5). They were better recognized than the pentasaccharide best mimicking *S. flexneri* 5a O-Ag (IC_{50} in the millimolar range) by at least one of the mIgAs used for selection. However, as outlined previously for other systems (17, 82, 83) and observed here for p115 and p100c, but not for p22, most selected peptides could discriminate between the two mIgAs used for selection. This is in agreement with the assumption that anti-polysaccharide mAbs may not necessarily recognize a single antigen topography. In line with previous work (83), it was thus hypothesized that peptide mimics reacting with a panel of anti-O-SP-specific mAbs would have a better potential to act as mimotopes than those with a strong discriminating potential. However, as observed by others (18), our data do not support this hypothesis. Indeed, among the three sequences selected for the study, discriminating p115 and p100c behave as mimotopes, whereas p22, recognized by both mIgAs, is only a mimic of *S. flexneri* 5a O-SP. Besides, considering the high affinity of p22 for mIgA C5 ($IC_{50} \sim 30$ nM), our model fits to others, such as that on *Cryptococcus neoformans* (18, 84) and that on *N. meningococcus* C (30), suggesting that commonly used parameters for selecting peptide mimicking polysaccharide antigens, such as high-affinity binding to mAb, are not predictive of the ability of the selected peptides to act as mimotopes. Indeed, based on x-ray analysis, several lines of evidence support the idea that peptide binding to an anti-polysaccharide mAb may differ significantly from that of the natural antigen. On one hand, data on the dodecapeptide PA1 mimicking *C. neoformans* CPS suggest poor steric complementarity between PA1 and the heavy chain of the mAb used for selection, which may explain why PA1 acts only as a partial mimotope (20). On the other hand, an octapeptide functional mimic of *S. flexneri* serotype Y O-SP was found to complement the shape of the groove-type binding site of mAb SYA/J6, used for selection, much better than the ABCDA′ pentasaccharide fragment of the O-SP (21). However, the peptide does not fully complement the deep pocket located in the center of the groove and occupied by rhamnose C upon binding of ABCDA′. This may explain, at least in part, the poor ability of the octapeptide to behave as an immunogenic mimic (9).

Not surprisingly, although the three peptides do not share any consensus sequence, the conformations they adopt in their free form encompass many rapidly interconverting conformers with short internal sequences spending long lifetimes organized in turn like motifs. Although p22 was found much more flexible than p115 or p100c, all three peptides adopted β-turn conformations, either of nonclassified type or of type I. This appears to be a rather common conformational feature for short peptides representative of antigenic regions of proteins (85) or polysaccharide antigens such as group A *Streptococcus* CP (9) and group B *Streptococcus* CP (38). Indeed, it has been suggested that a β-turn allows appropriate exposure of side chain residues for optimal fit within the mAb combining site. Most interestingly, in the later example, peptide FDTGAFDPDWPA, a molecular mimotope of the CPS, was earlier thought to adopt a nonrandom coil conformation in aqueous solution assimilated to a nascent helix that could potentially mimic the extended helical form of the natural carbohydrate epitope (29). This

discrepancy underscores the high complexity of conformational studies dealing with short peptides. The relative heterogeneity of β-turn types adopted by p115, p100c, and p22 in the free form is completely lost in the bound form, as the three peptides adopt a type II β-turn conformation, which appears to be crucial for binding independently of the involved mAb. Thus, the lack of consensus sequence among the selected peptides seems to be compensated by structural consensus induced upon fitting to the mAb combining sites. Moreover, the type II β-turn structure starts from a proline (Pro[3] and Pro[4], respectively) and ends with an alanine (Ala[6] and Ala[7], respectively) for both p115 and p100c, underscoring the partial structural resemblance between the two peptides. Major contributions of the p115-turn to binding involve aromatic Trp[5] and cyclic Pro[4], whereas hydrophobic Leu[5] was the residue most involved in mAb binding to the p100c-turn. p22 differs notably from p115 and p100c because it has no proline. In this case, aromatic His[3] and Phe[4] together with hydrophobic Leu[5] are the major turn components contributing to binding independently of the mAb. Noteworthy, additional residues do not seem to be engaged in mAb recognition, which may explain the ability of p22 to bind the two mIgAs. On the contrary, going from His[1] to Ala[9], p115 binding to mIgA C5 necessitates that most residues along the peptide chain, especially those at the N terminus, make specific contacts with the combining site. Similarly, residues at the N terminus of p100c appear critical for peptide binding to mIgA I3. In particular, the two docking models obtained for p100c interacting with mIgA I3 reveal a salt bridge formed between the peptide Lys[3] residue and the residue Asp[92] within the CDR H3 loop, similarly to those observed between rhamnose A or glucose E and Asp[92] or Asp[91] of the mIgA CDR H3 loop, respectively, upon DA(E)BC binding. Although not probed at this stage, analogous ionic contributions to peptide-mAb interactions may be anticipated because all selected peptides share basic residues. However, available data suggest that independently of the peptide mimic under study, all mIgA-peptide interactions derived mostly from the direct contact of peptide aromatic residues and methyl groups with the mAb-binding site, suggesting that recognition was basically driven by hydrophobic and van der Waals contacts. In that matter, data provided for the *S. flexneri* 5a system fully support previous observations made for other models implicating peptides mimicking polysaccharide antigens in complex with specific mAbs (11).

In addition, all data reported here strongly emphasize the crucial role played by the type II β-turn topology in governing molecular mimicry of *S. flexneri* 5a O-antigen. Most interestingly, superimposition of family of conformations obtained for bound p22 with this obtained for bound DA(E)BC-OMe shows that the type II β-turn in the peptide seems to mimic the nascent helicoidal shape of the oligosaccharide main chain with the aromatic ring of Phe[4] having the same orientation as the crucial branched glucose E (Fig. 11). This is in agreement with previous observations showing that aromatic amino acids are considered as ideal residues for mimicking glycan side chain structures (69, 86) and that β-turn/extended structures may be accurate conformational mimics of helices (87, 88). Yet, except for the number of residues involved, discriminating between the binding modes of the three peptides remains difficult. Thus, based on binding complementarity only, rules governing the selection of potent *S. flexneri* 5a O-Ag mimotopes remain undisclosed. Moreover, our data emphasize that the rational design of peptides mimicking the immunological properties of polysaccharides remains a challenge (89). Because investigating the peptide binding features left several unanswered questions, the behavior of the free peptides in solution was analyzed more closely. None of the free peptides adopt the required type II β-turn conformation fitting in the mAb combining sites. However, they are somehow predisposed to conformational reorganization for binding. More importantly, p115 bearing Pro[3] and Pro[4] both

---

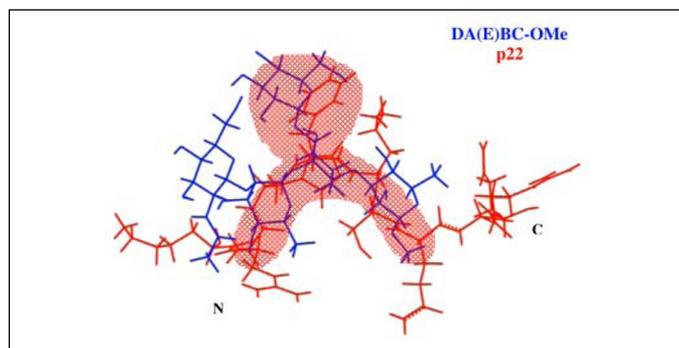[5] V. Marcel-Peyre and A. Phalipon, unpublished data.

FIGURE 11. **Potential conformational mimetism of the peptide p22 in relation to the pentasaccharide DA(E)BC-OMe.** The figure shows superimposition of the p22 lowest energy structure with that of the DA(E)BC-OMe. Structural elements showing the potential conformational mimetism of the peptide in relation to the oligosaccharide are shaded in *pink*.

involved in a turn and p100c being cyclic are both highly constrained, whereas p22 adopting a poorly stabilized nonclassified turn is much more flexible. Thus, our data suggest that the pre-organized conformation adopted by the free peptide is critical for efficiency as a mimotope. It is hypothesized that, besides the number of contacts with the mAb involved in binding, it may be especially important that the free peptides have a stable structure closely resembling that of the mAb-bound conformation (20, 89). Along this line as exemplified with p22, one of the possible explanations for the failure of some peptide mimics to induce a potent anti-LPS immune response is the limited ability of small free peptides to adopt the stable conformations necessary for functional mimicry. As a consequence, the immune response induced is broadened resulting in the induction of low titers of Abs exhibiting the required specificity. To our knowledge, a crucial issue for the development of mimotope-based vaccines remains unanswered, that is: what is the acceptable ability of polysaccharide-peptide mimics to induce cross-reactive antibodies? In other words, what is an acceptable conformational flexibility for the free peptide mimics? Ideally if a monovalent vaccine is the target, the range of accessible conformations should match those of the native antigen only. In that case, induction of cross-reactive Ab would be seen as a disadvantage, because as mentioned above the level of specific Ab is consequently lowered. More importantly, the risk of inducing an Ab response directed against self-antigens may be increased. However, by allowing cross-protection against different serotypes of a given bacterial species, cross-reactivity related to controlled flexibility may constitute an advantage if the development of multivalent vaccines is envisioned. This issue has to be further investigated.

In conclusion, our work brings new data that contribute to a better understanding of molecular mimicry of polysaccharide antigens by mimotopes. Encouraging data demonstrating the feasibility of using mimotopes as surrogates of native antigens for the induction of protective immune responses have been provided in the last 10 years. However, major breakthroughs are still needed to further establish the rules governing the molecular mimicry of polysaccharide antigens by peptides. Those should help the future design of efficient mimotope-based vaccines.

REFERENCES

1. MacLeod, C. M., Hodges, R. G., Heidelberg, M., and Bernhard, W. G. (1945) *J. Exp. Med.* **82,** 445–465
2. Roy, R. (2004) *Drug Discovery Today: Technologies* **1,** 327–336
3. Goebel, H. H., Ikeda, K., Schulz, F., Burck, U., and Kohlschutter, A. (1981) *Acta Neuropathol.* **55,** 247–249
4. Pozsgay, V., Chu, C., Pannell, L., Wolfe, J., Robbins, J. B., and Schneerson, R. (1999) *Proc. Natl. Acad. Sci. U. S. A.* **96,** 5194–5197
5. Peeters, C. C., Evenberg, D., Hoogerhout, P., Kayhty, H., Saarinen, L., van Boeckel, C. A., van der Marel, G. A., van Boom, J. H., and Poolman, J. T. (1992) *Infect. Immun.* **60,** 1826–1833
6. Verez-Bencomo, V., Fernandez-Santana, V., Hardy, E., Toledo, M. E., Rodriguez, M. C., Heynngnezz, L., Rodriguez, A., Baly, A., Herrera, L., Izquierdo, M., Villar, A., Valdes, Y., Cosme, K., Deler, M. L., Montane, M., Garcia, E., Ramos, A., Aguilar, A., Medina, E., Torano, G., Sosa, I., Hernandez, I., Martinez, R., Muzachio, A., Carmenates, A., Costa, L., Cardoso, F., Campa, C., Diaz, M., and Roy, R. (2004) *Science* **305,** 522–525
7. Stein, H., Gatter, K. C., Heryet, A., and Mason, D. Y. (1984) *Lancet* **2,** 71–73
8. Pirofski, L. A. (2001) *Trends Microbiol.* **9,** 445–451
9. Johnson, M. A., Rotondo, A., and Pinto, B. M. (2002) *Biochemistry* **41,** 2149–2157
10. Monzavi-Karbassi, B., Cunto-Amesty, G., Luo, P., and Kieber-Emmons, T. (2002) *Trends Biotechnol.* **20,** 207–214
11. Luo, P., Agadjanyan, M., Qiu, J., Westerink, M. A., Steplewski, Z., and Kieber-Emmons, T. (1998) *Mol. Immunol.* **35,** 865–879
12. Cunto-Amesty, G., Dam, T. K., Luo, P., Monzavi-Karbassi, B., Brewer, C. F., Van Cott, T. C., and Kieber-Emmons, T. (2001) *J. Biol. Chem.* **276,** 30490–30498
13. Fleuridor, R., Lees, A., and Pirofski, L. (2001) *J. Immunol.* **166,** 1087–1096
14. Lesinski, G. B., and Westerink, M. A. (2001) *J. Microbiol. Methods* **47,** 135–149
15. Maitta, R. W., Datta, K., Lees, A., Belouski, S. S., and Pirofski, L. A. (2004) *Infect. Immun.* **72,** 196–208
16. Buchwald, U. K., Lees, A., Steinitz, M., and Pirofski, L. A. (2005) *Infect. Immun.* **73,** 325–333
17. Harris, S. L., Craig, L., Mehroke, J. S., Rashed, M., Zwick, M. B., Kenar, K., Toone, E. J., Greenspan, N., Auzanneau, F. I., Marino-Albernas, J. R., Pinto, B. M., and Scott, J. K. (1997) *Proc. Natl. Acad. Sci. U. S. A.* **94,** 2454–2459
18. Valadon, P., Nussbaum, G., Oh, J., and Scharff, M. D. (1998) *J. Immunol.* **161,** 1829–1836
19. Cunto-Amesty, G., Luo, P., Monzavi-Karbassi, B., Lees, A., and Kieber-Emmons, T. (2001) *Vaccine* **19,** 2361–2368
20. Young, A. C., Valadon, P., Casadevall, A., Scharff, M. D., and Sacchettini, J. C. (1997) *J. Mol. Biol.* **274,** 622–634
21. Vyas, N. K., Vyas, M. N., Chervenak, M. C., Bundle, D. R., Pinto, B. M., and Quiocho, F. A. (2003) *Proc. Natl. Acad. Sci. U. S. A.* **100,** 15023–15028
22. Johnson, M. A., and Pinto, B. M. (2004) *Carbohydr. Res.* **339,** 907–928
23. Kotloff, K. L., Winickoff, J. P., Ivanoff, B., Clemens, J. D., Swerdlow, D. L., Sansonetti, P. J., Adak, G. K., and Levine, M. M. (1999) *Bull. W.H.O.* **77,** 651–666
24. Phalipon, A., and Sansonetti, P. J. (2003) *Crit. Rev. Immunol.* **23,** 371–401
25. Ashkenazi, S., Passwell, J. H., Harlev, E., Miron, D., Dagan, R., Farzan, N., Ramon, R., Majadly, F., Bryla, D. A., Karpas, A. B., Robbins, J. B., and Schneerson, R. (1999) *J. Infect. Dis.* **179,** 1565–1568
26. Wright, K., Guerreiro, C., Laurent, I., Baleux, F., and Mulard, L. A. (2004) *Org. Biomol. Chem.* **2,** 1518–1527
27. Belot, F., Guerreiro, C., Baleux, F., and Mulard, L. A. (2005) *Chemistry* **11,** 1625–1635
28. Phalipon, A., Folgori, A., Arondel, J., Sgaramella, G., Fortugno, P., Cortese, R., Sansonetti, P. J., and Felici, F. (1997) *Eur. J. Immunol.* **27,** 2620–2625
29. Pincus, S. H., Lepage, S. R., Jung, R. F., Massey, J. G., and Jaseja, M. (2001) *Int. Rev. Immunol.* **20,** 221–227
30. Prinz, D. M., Smithson, S. L., and Westerink, M. A. (2004) *J. Immunol. Methods* **285,** 1–14
31. Lindberg, A. A., Cam, P. D., Chan, N., Phu, L. K., Trach, D. D., Lindberg, G., Karlsson, K., Karnell, A., and Ekwall, E. (1991) *Rev. Infect. Dis.* **13,** Suppl. 4, 231–237
32. Mulard, L. A., and Ughetto-Monfrin, J. (2000) *J. Carbohydr. Chem.* **19,** 193–220
33. Clement, M. J., Imberty, A., Phalipon, A., Perez, S., Simenel, C., Mulard, L. A., and Delepierre, M. (2003) *J. Biol. Chem.* **278,** 47928–47936
34. Clore, G. M., and Gronenborn, A. M. (1982) *J. Magn. Reson.* **48,** 402–417
35. Clore, G. M., and Gronenborn, A. M. (1983) *J. Magn. Reson.* **53,** 423–442
36. Mayer, M., and Meyer, B. (1999) *Angew. Chem. Int. Ed.* **38,** 1784–1788
37. Johnson, M. A., and Pinto, B. M. (2002) *J. Am. Chem. Soc.* **124,** 15368–15374
38. Johnson, M. A., Jaseja, M., Zou, W., Jennings, H. J., Copie, V., Pinto, B. M., and Pincus, S. H. (2003) *J. Biol. Chem.* **278,** 24740–24752
39. Johnson, M. A., and Pinto, B. M. (2004) *Bioorg. Med. Chem.* **12,** 295–300
40. Mulard, L. A., Clément, M.-J., Segat-Dioury, F., and Delepierre, M. (2002) *Tetrahedron* **58,** 2593–2604
41. Phalipon, A., Kaufmann, M., Michetti, P., Cavaillon, J. M., Huerre, M., Sansonetti, P., and Kraehenbuhl, J. P. (1995) *J. Exp. Med.* **182,** 769–778

42. Rance, M., Sorensen, O. W., Bodenhausen, G., Wagner, G., Ernst, R. R., and Wuthrich, K. (1983) *Biochem. Biophys. Res. Commun.* **117,** 479–485

43. Griesinger, C., Otting, G., Wüthrich, K., and Ernst, R. R. (1988) *J. Am. Chem. Soc.* **110,** 7870–7872

44. Kessler, H., Griesinger, C., Kerssebaum, R., Wagner, K., and Ernst, R. R. (1987) *J. Am. Chem. Soc.* **109,** 607–609

45. Piotto, M., Saudek, V., and Sklenar, V. (1992) *J. Biomol. NMR* **2,** 661–665

46. States, D. J., Haberkorn, R. A., and Ruben, D. J. (1982) *J. Magn. Reson.* **48,** 286–292

47. Jimenez-Barbero, J., and Peters, T. (eds) (2002) *NMR Spectroscopy of Glycoconjugates*, pp. 289–307, Wiley-VCH, New York

48. Herfurth, L., Weimar, T., and Peters, T. (2000) *Angew. Chem. Int. Ed. Engl.* **39,** 2097–2099

49. Baleja, J., Moult, J., and Sykes, B. D. (1990) *J. Magn. Reson.* **87,** 375–384

50. Wüthrich, K. (1986) *NMR of Proteins and Nucleic Acids*, John Wiley & Sons, Inc., New York

51. Pardi, A., Billeter, M., and Wuthrich, K. (1984) *J. Mol. Biol.* **180,** 741–751

52. Guntert, P., Mumenthaler, C., and Wuthrich, K. (1997) *J. Mol. Biol.* **273,** 283–298

53. Koradi, R., Billeter, M., and Wuthrich, K. (1996) *J. Mol. Graphics* **14,** 51–55

54. Altschul, S. F., Madden, T. L., Schaffer, A. A., Zhang, J., Zhang, Z., Miller, W., and Lipman, D. J. (1997) *Nucleic Acids Res.* **25,** 3389–3402

55. Berman, H. M., Westbrook, J., Feng, Z., Gilliland, G., Bhat, T. N., Weissig, H., Shindyalov, I. N., and Bourne, P. E. (2000) *Nucleic Acids Res.* **28,** 235–242

56. Blundell, T., Carney, D., Gardner, S., Hayes, F., Howlin, B., Hubbard, T., Overington, J., Singh, D. A., Sibanda, B. L., and Sutcliffe, M. (1988) *Eur. J. Biochem.* **172,** 513–520

57. Clark, M., Cramer, R. D. I., and van den Opdenbosch, N. (1989) *J. Comput. Chem.* **10,** 982–1012

58. Laskowski, R., MacArthur, M., Moss, D., and Thornton, J. (1993) *J. Appl. Crystallogr.* **26,** 283–291

59. Morris, G. M., Goodsell, D. S., Halliday, R. S., Huey, R., Hart, W. E., Belew, R. K., and Olson, A. J. (1998) *J. Comput. Chem.* **19,** 1639–1662

60. Imberty, A., Bettler, E., Karababa, M., Mazeau, K., Petrova, P., and Pérez, S. (1999) in *Perspectives in Structural Biology* (Vijayan, M., Yathindra, N., and Kolaskar, A. S., eds) pp. 392–409, Indian Academy of Sciences and Universities Press, Hyderabad

61. Rose, G. D., Gierasch, L. M., and Smith, J. A. (1985) *Adv. Protein Chem.* **37,** 1–109

62. Wilmot, C. M., and Thornton, J. M. (1988) *J. Mol. Biol.* **203,** 221–232

63. Pokkuluri, P. R., Bouthillier, F., Li, Y., Kuderova, A., Lee, J., and Cygler, M. (1994) *J. Mol. Biol.* **243,** 283–297

64. Herron, J. N., He, X. M., Ballard, D. W., Blier, P. R., Pace, P. E., Bothwell, A. L., Voss, E. W., Jr., and Edmundson, A. B. (1991) *Proteins* **11,** 159–175

65. Romesberg, F. E., Spiller, B., Schultz, P. G., and Stevens, R. C. (1998) *Science* **279,** 1929–1933

66. Tulip, W. R., Harley, V. R., Webster, R. G., and Novotny, J. (1994) *Biochemistry* **33,** 7986–7997

67. Shoham, M. (1993) *J. Mol. Biol.* **232,** 1169–1175

68. Agadjanyan, M., Luo, P., Westerink, M. A., Carey, L. A., Hutchins, W., Steplewski, Z.,

69. Dinglasan, R. R., Porter-Kelley, J. M., Alam, U., and Azad, A. F. (2005) *Vaccine* **23,** 2717–2724

70. Bernardi, A., Potenza, D., Capelli, A. M., Garcia-Herrero, A., Canada, F. J., and Jimenez-Barbero, J. (2002) *Chemistry* **8,** 4597–4612

71. Bundle, D. R., Eichler, E., Gidney, M. A., Meldal, M., Ragauskas, A., Sigurskjold, B. W., Sinnott, B., Watson, D. C., Yaguchi, M., and Young, N. M. (1994) *Biochemistry* **33,** 5172–5182

72. Vyas, N. K., Vyas, M. N., Chervenak, M. C., Johnson, M. A., Pinto, B. M., Bundle, D. R., and Quiocho, F. A. (2002) *Biochemistry* **41,** 13575–13586

73. Bock, K., Josephson, S., and Bundle, D. R. (1982) *J. Chem. Soc. Perkins Trans.* **2,** 59–70

74. Kreis, U. (1997) *J. Mol. Struct. (Theochem)* **395–396,** 389–409

75. Cisar, J., Kabat, E. A., Dorner, M. M., and Liao, J. (1975) *J. Exp. Med.* **142,** 435–459

76. Pitner, J. B., Beyer, W. F., Venetta, T. M., Nycz, C., Mitchell, M. J., Harris, S. L., Marino-Albernas, J. R., Auzanneau, F. I., Forooghian, F., and Pinto, B. M. (2000) *Carbohydr. Res.* **324,** 17–29

77. Padlan, E. A. (1990) *Proteins* **7,** 112–124

78. Bernardi, A., Arosio, D., Potenza, D., Sanchez-Medina, I., Mari, S., Canada, F. J., and Jimenez-Barbero, J. (2004) *Chemistry* **10,** 4395–4406

79. Oomen, R. P., Young, N. M., and Bundle, D. R. (1991) *Protein Eng.* **4,** 427–433

80. Rose, D. R., Przybylska, M., To, R. J., Kayden, C. S., Oomen, R. P., Vorberg, E., Young, N. M., and Bundle, D. R. (1993) *Protein Sci.* **2,** 1106–1113

81. Lauvrak, V., Berntzen, G., Heggelund, U., Herstad, T. K., Sandin, R. H., Dalseg, R., Rosenqvist, E., Sandlie, I., and Michaelsen, T. E. (2004) *Scand. J. Immunol.* **59,** 373–384

82. Valadon, P., Nussbaum, G., Boyd, L. F., Margulies, D. H., and Scharff, M. D. (1996) *J. Mol. Biol.* **261,** 11–22

83. Pincus, S. H., Smith, M. J., Jennings, H. J., Burritt, J. B., and Glee, P. M. (1998) *J. Immunol.* **160,** 293–298

84. Beenhouwer, D. O., May, R. J., Valadon, P., and Scharff, M. D. (2002) *J. Immunol.* **169,** 6992–6999

85. Dyson, H. J., Rance, M., Houghten, R. A., Lerner, R. A., and Wright, P. E. (1988) *J. Mol. Biol.* **201,** 161–200

86. Monzavi-Karbassi, B., Shamloo, S., Kieber-Emmons, M., Jousheghany, F., Luo, P., Lin, K. Y., Cunto-Amesty, G., Weiner, D. B., and Kieber-Emmons, T. (2003) *Vaccine* **21,** 753–760

87. Monfardini, C., Kieber-Emmons, T., VonFeldt, J. M., Godillot, A. P., Voet, D., Weiner, D. B., and Williams, W. V. (1996) *Proc. Assoc. Am. Physicians* **108,** 420–431

88. Mer, G., Kellenberger, E., and Lefevre, J. F. (1998) *J. Mol. Biol.* **281,** 235–240

89. Johnson, M. A., Eniade, A. A., and Pinto, B. M. (2003) *Bioorg. Med. Chem.* **11,** 781–788

90. Wishart, D. S., Bigam, C. G., Holm, A., Hodges, R. S., and Sykes, B. D. (1995) *J. Biomol. NMR* **5,** 67–81

91. Wilmot, C. M., and Thornton, J. M. (1990) *Protein Eng.* **3,** 479–493

92. Richardson, J. S. (1981) *Adv. Protein Chem.* **34,** 167–339

Weiner, D. B., and Kieber-Emmons, T. (1997) *Nat. Biotechnol.* **15,** 547–551